Ferroportin 3 is a dual-targeted mitochondrial/chloroplast iron exporter necessary for iron homeostasis in Arabidopsis

Leah J. Kim[a], Kaitlyn M. Tsuyuki[a, 4], Fengling Hu[a, 4], Emily Y. Park[a, 4], Jingwen Zhang[a, 4], Jennifer Gallegos Iraheta[a], Ju-Chen Chia[b], Rong Huang[c], Avery E. Tucker[a], Madeline Clyne[a], Claire Castellano[a], Angie Kim[a], Daniel D. Chung[a], Christopher T. DaVeiga[a], Elizabeth M. Parsons[a], Olena K. Vatamaniuk[b], Jeeyon Jeong[a, 2, 3]

[a]Department of Biology, Amherst College, Amherst, Massachusetts 01002

[b]Soil and Crop Sciences Section, School of Integrative Plant Science, Cornell University, Ithaca, New York 14853

[c]Cornell High Energy Synchrotron Source, Ithaca, New York 14853

Running title: A mitochondrial ferroportin in Arabidopsis

Keywords: Iron, Ferroportin, Mitochondria, Chloroplast, Arabidopsis, Transport

One sentence summary: FPN3 is an iron exporter dual-targeted to the mitochondria and plastids and is required for optimal growth under iron deficiency.

[1]This work was supported by the National Science Foundation (NSF) grant to JJ (IOS-1754969) and OKV (IOS-1656321), the Gregory S. Call Undergraduate Research Program (LK, KT, EYP, FH, JG, MC, AK, DC, CD, EMP), Doelling Undergraduate Research Fund (LK, KT, EYP, JG, AK, DC, CD, EMP), Schupf Scholars Program (JZ), and the Sarles Fellowship (MC). The transmission electron microscopy was supported by the National Center for Research Resources

award (SI0OD021580) to the UMass Medical School Electron Microscopy Facility. The authors are solely responsible for the content of this paper and do not necessarily represent the official views of the National Center for Research Resources, National Institutes of Health, or NSF. CHESS is supported by the NSF and NIH/NIGMS via NSF Award DMR-1332208.

[2]Author for contact: jjeong@amherst.edu

[3]Senior author.

[4]These authors have equally contributed to the manuscript.

J.J. conceived the idea and supervised the study, J.J wrote the article with contributions of L.K., K.T., F.H., E.Y.P., J.Z., and J.G.; Microscopy experiments were conducted by L.K., E.Y.P., and J.J; L.K., F.H., J.Z., J.G., M.C., and C.C. performed the yeast experiments; L.K., J.G., and E.M.P. conducted the GUS assays; L.K., K.T., E.Y.P., F. H., and J.Z., conducted gene expression analyses; L.K. and C.D. carried out the plant growth assays; F.H., A.T., K.T., A.K., and D.C. performed cloning and generated transgenic lines; L.K. isolated chloroplasts; L.K. and K.T. isolated mitochondria; L.K. and K.T. conducted Western blots and ICP-MS; J-C.C. and R.H. conducted SXRF imaging; O.K.V. supervised the SXRF experiments; all authors read and approved the manuscript.

ABSTRACT

Mitochondria and chloroplasts are organelles with high iron demand that are highly susceptible to iron-induced oxidative stress. Despite the necessity of strict iron regulation in these organelles, much remains unknown about mitochondrial and chloroplast iron transport in plants. Here, we show that Arabidopsis Ferroportin 3 (FPN3) is an iron exporter dual-targeted to mitochondria and chloroplasts. *FPN3* is expressed in shoots regardless of iron conditions, but is iron-regulated in the roots. *fpn3* mutants cannot grow as well as wild type under iron-deficient conditions and shoot iron levels are reduced in *fpn3* mutants compared to wild type. Analyses of iron homeostasis gene expression in *fpn3* mutants and ICP-MS measurements suggest that iron levels in the mitochondria and chloroplasts are increased relative to wild type, consistent with the proposed role of FPN3 as a mitochondrial/plastid iron exporter. In iron deficient *fpn3* mutants, abnormal mitochondrial ultrastructure was observed, whereas chloroplast ultrastructure was not affected, implying that FPN3 plays a critical role in iron metabolism in mitochondria. Overall, we propose that FPN3 is crucial for iron homeostasis.

INTRODUCTION

Iron serves as a critical redox cofactor in vital cellular processes. Nevertheless, excess or improperly regulated iron can cause deleterious effects by generating hydroxyl radicals via the Fenton reaction (Halliwell and Gutteridge, 1992). Therefore, iron homeostasis must be tightly maintained in all organisms, including plants. As photosynthetic organisms, plants use iron as an essential cofactor in both respiration and photosynthesis. At the same time, plants cells must regulate iron to ensure adequate supply while avoiding oxidative stress (Shcolnick and Keren, 2006). Despite being an abundant element in the soil, iron is one of the most limiting nutrients for plant growth – it has extremely low bioavailability under aerobic conditions at neutral or alkaline pH (Marschner, 2012; Colombo et al., 2014). Iron homeostasis in plants is of particular interest, because understanding its mechanisms will provide insights to improving agriculture and human health (Vasconcelos et al., 2017).

Dicots acquire iron by a reduction-based mechanism that is induced under iron deficiency (Brumbarova et al., 2015; Connorton et al., 2017; Jeong et al., 2017; Kobayashi et al., 2018). Ferric chelates in the rhizosphere are solubilized by the release of protons (Santi and Schmidt, 2009) and reduced to ferrous iron by FERRIC REDUCTASE OXIDASE 2 (FRO2) (Robinson et al., 1999). Coumarins released from iron-deficient roots are considered to aid this process as well (Fourcroy et al., 2014; Schmidt et al., 2014; Clemens and Weber, 2016). Ferrous iron is then transported into the root via IRON-REGULATED TRANSPORTER 1 (IRT1) (Connolly et al., 2002; Varotto et al., 2002; Vert et al., 2002). Once iron reaches the root vasculature, it is loaded into the xylem by FERROPORTIN 1 (FPN1) (Morrissey et al., 2009) and chelated with citrate, which is transported into the xylem by the FERRIC REDUCTASE DEFECTIVE 3 (FRD3) transporter (Durrett et al., 2007). The iron-citrate complex is then translocated to shoots. For

lateral translocation in shoots, iron-nicotianamine (NA) complexes are formed and translocated from leaves to seeds via the phloem by YELLOW STRIPE-LIKE (YSL) family members (DiDonato et al., 2004; Schaaf et al., 2005; Waters et al., 2006). Two YSL members, YSL1 and YSL3, were shown to regulate long-distance iron-deficiency signals from shoots (Kumar et al., 2017). Oligopeptide transporter 3 (OPT3) also plays a role in transmitting shoot-to-root iron signals and regulates the redistribution of iron from source to sink tissues, such as from old leaves to seeds or to developing tissues (Stacey et al., 2008; Mendoza-Cózatl et al., 2014; Zhai et al., 2014). Iron is also loaded into the seeds via YSL1 and YSL3 (Le Jean et al., 2005; Waters et al., 2006).

In addition to iron acquisition and its distribution between tissues, iron trafficking across subcellular compartments is crucial for proper iron homeostasis. In particular, chloroplasts and mitochondria need a substantial amount of iron; many components of the photosynthetic and respiratory electron transport chains use iron as a cofactor. Fe-S cluster assembly occurs in these organelles and heme biosynthesis occurs in plastids (Masuda et al., 2003; Tanaka et al., 2011). Proteins involved in the last stage of heme biosynthesis are also present in mitochondria (Balk and Schaedler, 2014). Chloroplasts are the most iron-rich organelle in plant cells and accounts for 60-80% of iron found in a leaf cell (Terry and Low, 1982; Shikanai et al., 2003). Meanwhile, in the mitochondria, iron is the major micronutrient present with a molar ratio of 26:8:6:1 for Fe:Zn:Cu:Mn (Tan et al., 2010). Mitochondria and chloroplasts are also highly susceptible to oxidative stress due to reactive oxygen species (ROS) generated by the electron transport chain. It has been shown that the iron sequestering protein ferritin is present in mitochondria, as well as in plastids, and helps to prevent iron-induced oxidative stress (Zancani et al., 2004; Briat et al., 2010; Tarantino et al., 2010a).

Iron transport in mitochondria and chloroplasts is not as well understood as the mechanisms of iron acquisition in the roots, but molecular and physiological studies have been gradually contributing to understanding iron regulation in chloroplasts and mitochondria. In chloroplasts, physiological studies suggest that ferric chelates move across the outer membrane (Bughio et al., 1997; Solti et al., 2012; Müller et al., 2019), but ferrous iron is imported into chloroplasts across the inner membrane (Bughio et al., 1997; Shingles et al., 2002). The ferric chelate reductase, FRO7, reduces iron for chloroplast iron acquisition (Jeong et al., 2008), and PERMEASE IN CHLOROPLAST 1 (PIC1) mediates iron transport into chloroplasts via interaction with NiCo (Duy et al., 2007; Duy et al., 2011). A recent study in Brassica napus proposes that NiCo may also be involved in iron sensing or iron release from chloroplasts (Pham et al., 2020). The Arabidopsis MitoFerrinLike1 (Mfl1) has also been reported to import iron into chloroplasts (Tarantino et al., 2011). In addition, ATP-binding cassette transporters, ABCI10, NAP14/ABCI11, and ABCI12, may also contribute to iron uptake into chloroplasts (Shimoni-Shor et al., 2010; Voith von Voithenberg et al., 2019). YSL4 and YSL6 have been reported to efflux iron-NA complexes from the chloroplasts (Divol et al., 2013). However, both transporters were also identified in the tonoplast proteome (Jaquinod et al., 2007) and were targeted to the vacuolar and intracellular membranes (Conte et al., 2013). ZmFRD4 was reported as a potential thylakoid iron importer in maize, although direct evidence for iron transport remains to be found (Zhang et al., 2017).

In the mitochondria, a mitoferrin ortholog from rice, MITOCHONDRIAL IRON TRANSPORTER 1 (MIT1), was identified as a mitochondrial iron importer (Bashir et al., 2011). Two Arabidopsis mitoferrin orthologs, MIT1 and MIT2, have recently been reported as mitochondrial iron importers that mediate cellular iron homeostasis and are essential for

embryogenesis (Jain et al., 2019). In *Cucumis sativus*, a cation diffusion facilitator (CDF) family member, METAL TRANSPORT PROTEIN 7, was shown to import mitochondrial iron (Migocka et al., 2018). A reduction-based mechanism might be involved in moving iron in and out of mitochondria, because ferric chelate reductases, FRO3 and FRO8, are localized to the mitochondria in Arabidopsis (Heazlewood et al., 2004; Jeong and Connolly, 2009). The two mitochondrial FROs are likely to play non-overlapping roles, as *FRO3* is induced by iron deficiency, whereas *FRO8* is not iron-regulated (Mukherjee et al., 2006; Jeong and Connolly, 2009).

In this study, we investigated an Arabidopsis FPN family member, FPN3/IREG3. FPNs, also known as solute carrier (SCL) group 40A1 and IRON REGULATED (IREG) transporters, share a conserved FPN motif and efflux iron from the cytoplasm (Drakesmith et al., 2015). In animals, FPNs are found in cells that play critical roles in supplying iron, such as intestinal cells. While animal species have only one FPN, multiple FPN paralogs are present within most plant species. In Arabidopsis, three FPN family members were identified based on phylogenetic analysis (Schaaf et al., 2006). FPN1/IREG1 (At2g38460) and FPN2/IREG2 (At5g03570) share 77 % identity, whereas FPN3/IREG3 (At5g26820) shares about 20% identity with FPN1 and FPN2 (Supplementary Figure 1). FPN1/IREG1 localizes to the plasma membrane of cells in the stele, where it loads iron into the vasculature for supply to the rest of the plant, and FPN2/IREG2 is localized on the vacuolar membrane to buffer cellular metal influx (Morrissey et al., 2009). Previously, FPN3/IREG3 was reported as Multiple Antibiotic Resistance 1 (MAR1), a chloroplast protein that allows antibiotics to opportunistically enter chloroplasts (Conte et al., 2009). While it was speculated that MAR1 may be involved in iron homeostasis, its potential role in iron regulation was not investigated. Here, we report that FPN3 is dual-targeted to

mitochondria and chloroplasts, and exports iron from these organelles. Furthermore, our study provides key evidence that suggests FPN3 plays critical role in iron homeostasis and its function is important in the mitochondria as represented by the drastic morphological changes in *fpn3* mitochondria under iron deficient conditions.

RESULTS

FPN3-GFP is dual-targeted to the mitochondria and plastids in Arabidopsis

To determine the subcellular localization of FPN3, we generated a C-terminal GFP fusion of FPN3 and expressed it in Arabidopsis mesophyll protoplasts. When co-expressed with a mitochondrial marker, *F_1-ATPaseγ-RFP* (Jin et al., 2003), the mitochondrial marker signal co-localized with FPN3-GFP, indicating that FPN3-GFP was targeted to the mitochondria (Figure 1A-D). In addition, we observed FPN3-GFP signal in the chloroplasts (Figure 1A-D). As an alternative approach to verify the localization of FPN3 in a background without chlorophyll autofluorescence, we generated transgenic Arabidopsis plants that stably express *FPN3-GFP* and examined the subcellular localization of FPN3-GFP in roots after staining with MitoTracker Red, a mitochondrial dye. In transgenic roots, FPN3-GFP signal co-localized with the fluorescence of MitoTracker Red (Figure 1E-G). In addition, we detected FPN3-GFP signal in areas that did not overlap with the mitochondrial staining (Figure 1E-G), which further suggested that FPN3-GPF might be dual-targeted.

To confirm the localization of FPN3-GFP in chloroplasts, we also generated transgenic Arabidopsis plants stably expressing both *FPN3-GFP* and *pt-RFP,* a plastid marker with the transit peptide of rubisco small subunit from tobacco fused to RFP (Nelson et al., 2007). We observed co-localization of FPN3-GFP with the plastid marker (Figure 1H-J), which was

consistent with the previous report by Conte et al. (2009) and our results from protoplasts transiently expressing FPN3-GFP (Figure 1A-D) . Overall, our results from both transient expression in protoplasts and stable transgenic lines confirm the plastid localization of FPN3-GFP and provide further evidence that FPN3 is dual-targeted.

Heterologously expressed *FPN3* is targeted to the mitochondria and likely exports iron from mitochondria in yeast

While the mechanism of iron transport by ferroportin transporters remains to be understood, structural modeling and *in vitro* assays with mutated variant FPNs identified three aspartate and one arginine residues of human FPN that are involved in iron binding and transport (Bonaccorsi di Patti et al., 2014). Sequence alignment of the FPN orthologs revealed that the residues critical for iron binding and transport in human FPN were also highly conserved in Arabidopsis FPN3, as well as the other Arabidopsis FPNs and those of zebrafish, mouse and bacteria (Supplementary Figure 1). Therefore, FPN3 is highly likely to transport ferrous iron, which is the substrate of FPNs in human, mouse, and zebrafish (Drakesmith et al., 2015). FPN family members identified to date transport iron *from* the cytoplasm. As metal transporters of the same family generally retain the direction of transport in respect to the cytoplasm, an organellar FPN is likely to transport iron into the organellar lumen. However, the endosymbiotic origin of mitochondria and chloroplasts (Yoon et al., 2004; Zimorski et al., 2014; Roger et al., 2017) suggests that FPN3 might be effluxing iron from its ancestral cytoplasm, i.e., from the organellar lumen into the eukaryotic cytoplasm.

To test FPN3 function at the cellular level and the directionality of its transport, we expressed *FPN3* in *Saccharomyces cerevisiae.* FPN3 was targeted to the mitochondria in yeast as

confirmed by FPN3-FLAG detected in mitochondrial fractions, identified based on the presence of the porin, a mitochondrial marker (Supplementary Figure 2). The mitochondrial localization of FPN3 in yeast is consistent with its subcellular localization to mitochondria and chloroplasts/plastids in plants, because chloroplast proteins can be targeted to the mitochondria when expressed in fungi (Hurt et al., 1986; Pfaller et al., 1989; Brink et al., 1994; Versaw and Harrison, 2002; Jeong et al., 2008).

Previous studies showed that Δ*mmt1/2*, which lack mitochondrial iron exporters, did not have a strong phenotype, but the deletion of *MMT1/2* in a Δ*ccc1* background, which lacks a vacuolar iron importer, resulted in a slighlty decreased sensitivity to high iron compared to Δ*ccc1* (Li et al., 2014). Additionally, Δ*ccc1*Δ*mmt1/2* cells expressing *MMT1/2* are highly sensitive to high iron due to increased cytosolic iron (Li et al., 2014). In the present study, we expressed *FPN3* in Δ*ccc1*Δ*mmt1/2* under high iron conditions to test if phenotypes similar to Δ*ccc1*Δ*mmt1/2* cells expressing *MMT1/2* would arise. Consistent with observations by Li et al. (2014), the expression of *MMT1/2* resulted in reduced growth in high iron (Figure 2A). The growth of Δ*ccc1*Δ*mmt1/2* expressing *FPN3* was decreased in high iron and approximated that of Δ*ccc1*Δ*mmt1/2* expressing *MMT1/2* (Figure 2A). This result suggests that FPN3 exports iron from the mitochondria (Figure 2A).

We also expressed *FPN3* in the *Δmrs3Δmrs4* yeast mutant, which lacks the mitochondrial iron importers, Mrs3 and Mrs4, to test if FPN3 is likely to import iron into mitochondria. The *Δmrs3Δmrs4* mutant does not have a strong iron phenotype, but exhibits increased sensitivity to oxidative stress compared to wild type cells (Foury and Roganti, 2002; Mühlenhoff et al., 2003). Expression of *FPN3* in *Δmrs3Δmrs4* did not rescue the oxidative stress sensitivity of

Δmrs3Δmrs4 (Supplementary Figure 3), which would be expected if *FPN3* were a mitochondrial iron importer. By contrast, *FPN3* expression exacerbated the phenotype, consistent with that of cells expressing *MMT1/2* (Supplementary Figure 3), suggesting that FPN3 is not likely to be importing iron into the mitochondria.

Based on the results from Δ*ccc1*Δ*mmt1/2* and *Δmrs3Δmrs4* cells expressing *FPN3* or *MMT1/2*, we hypothesized that FPN3 is a mitochondrial iron exporter. If FPN3 is exporting iron from the mitochondria, mitochondrial iron levels should be lower in cells overexpressing *FPN3*. To test this hypothesis, we measured the activity of aconitase in mitochondria to indirectly assess mitochondrial iron levels. Aconitase is a Fe-S enzyme involved in the tricarboxylic acid cycle, and its activity correlates with the availability of mitochondrial iron. For example, decreased aconitase activity has been detected in the yeast *Δmrs3/4* cells and rice plants defective in mitochondrial iron import (Foury and Roganti, 2002; Bashir et al., 2011). Although aconitase is present in the mitochondria and the cytosol, mitochondrial aconitase accounts for most of the cellular aconitase activity in yeast, and yeast cytosolic aconitase is not involved in regulating iron metabolism unlike in mammalian cells (Regev-Rudzki et al., 2005). Aconitase activity of cells expressing *FPN3* was similar to cells expressing *MMT1/2* and exhibited about 30% lower activity than that of the negative control with an empty vector (Figure 2B), suggesting that FPN3 is exporting iron from the mitochondria.

As an alternative approach to testing mitochondrial iron export by FPN3, we examined if cytosolic iron levels increased in cells expressing *FPN3*. We co-transformed *FPN3* or control plasmids along with a plasmid that expresses the bacterial gentisate 1,2-dioxygenase (GDO) in the yeast cytoplasm (Li et al., 2012) and measured GDO activity. GDO uses iron as a cofactor

and the activity of cytosolic GDO (c-GDO), which has been confirmed to localize to the cytoplasm in yeast, correlates with the amount of cytosolic iron. Thus, c-GDO can serve as an indicator of cytosolic iron levels in yeast (Li et al., 2012; Li et al., 2014). We detected significantly higher c-GDO activity in cells expressing *FPN3* or *MMT1/2*, whereas only background level activity was observed in cells with the empty vector control (Figure 2C). This result is consistent with our findings from yeast growth tests and aconitase activity assays (Figure 2A, B). Overall, our yeast results consistently supported the hypothesis that FPN3 is a mitochondrial iron exporter and is functionally analogous to Mmt1/2.

***FPN3* is expressed in the shoots, roots, flowers, and siliques, and is iron-regulated in roots**

To detect the expression of *FPN3* at the tissue level, we fused the promoter region of *FPN3* to the β-glucuronidase (GUS) reporter gene (*FPN3p-GUS*), transformed the construct into wild type Arabidopsis, and conducted GUS histochemical staining. *FPN3p-GUS* was expressed in shoots and roots of seedlings from an early stage, and in floral organs and siliques (Figure 3A-F), which was in agreement with *FPN3* expression data reported in multiple transcriptomics studies (Zimmermann et al., 2004; Schmid et al., 2005; Winter et al., 2007; Dinneny et al., 2008).

To determine whether *FPN3* expression is regulated by iron, we performed GUS staining with *FPN3p-GUS* plants grown under iron-deficient or iron-sufficient conditions. We detected stronger staining in roots of seedlings from iron-deficient medium than in roots from iron-sufficient medium, whereas *FPN3p-GUS* staining in the shoots was prominent under both conditions (Figure 3I-K). *FPN3p-GUS* expression in 1-day old seedlings exhibited similar patterns, with more intense staining in the roots of plants grown under iron-deficient conditions compared to plants from iron-sufficient conditions (Figure 3G, H). Staining in the shoots was

similar in both iron conditions. This observation corroborates our RT-qPCR results in which *FPN3* transcript level was approximately 4.5-fold higher in iron-deficient roots (Figure 3L), and is consistent with transcriptomics studies that reported higher steady state levels of *FPN3* transcripts in iron-deficient roots (Dinneny et al., 2008; Buckhout et al., 2009; Yang et al., 2010; Mai et al., 2016; Khan et al., 2018; Park et al., 2019). Meanwhile, constitutive expression of *FPN3* was detected in the shoots regardless of the iron status of the plant (Figure 3I, L).

FPN3 is iron-regulated primarily by local signals in roots

Studies with multiple plant species have revealed that two types of iron-deficiency signals regulate the iron-deficiency response in the roots: the local signal determined by the iron level in the rhizosphere, and the systemic, long distance signal based on the iron status of the shoots (Bienfait et al., 1987; Grusak and Pezeshgi, 1996; Vert et al., 2003; García et al., 2013).

The differential level of *FPN3* transcripts in roots and shoots prompted us to test if the iron-dependent *FPN3* accumulation in roots is regulated by a local or long-distance signal. Thus, we generated two lateral roots, or split roots, and each root was subjected to different iron growth conditions. The iron growth conditions for our split-root experiments were optimized based on the method by Kumar et al. (2017). Plants were grown under iron-deficient or iron-sufficient conditions for 3 days prior to the split media experiment and RNA was extracted from each side of the split root after 0, 6, or 12 hours after transfer (Figure 4A) for RT-qPCR. If *FPN3* level in the roots is regulated by a long-distance signal from the shoots, then *FPN3* expression is expected to be higher in both sides of the split roots of plants that were initially grown in iron deficient medium, regardless of the iron conditions for each side of the split roots. Our results revealed that, regardless of the initial growth conditions, significantly more *FPN3* transcripts accumulated in the split root subjected to iron-deficiency compared to its counterpart grown in

iron sufficient medium (Figure 4B). This suggests that the increased level of *FPN3* transcripts in iron deficient roots is primarily driven by the local iron conditions (Figure 4B). In the split root transferred from iron sufficient conditions to iron deficient conditions, we observed the greatest increase in *FPN3* transcript levels (Figure 4B). Meanwhile, between the split roots pre-treated under iron deficiency, only the split root subjected to an additional iron deficiency exhibited higher levels of *FPN3* over the time course tested. However, in the split-root transferred from iron sufficient to sufficient conditions, it was noted that there was a 2-fold increase in FPN3 transcript level (Figure 2). This observation suggests that systematic signal from the other split root may be involved. Overall, our split-root results suggest that *FPN3* expression in roots is regulated by the local iron status in the roots, but some systemic signaling may be involved as well.

Growth of *fpn3* mutants is reduced under iron deficiency

We then conducted phenotypic analyses with *fpn3* plants to understand the function of FPN3. Based on the increased *FPN3* expression in roots under iron deficiency (Figure 3I-L), we hypothesized that *fpn3* mutants might have less iron available for growth or development. To test this idea, we germinated two T-DNA insertion lines, *fpn3-1* and *fpn3-2*, which had drastically reduced levels of *FPN3* transcripts (Supplementary Figure 4) in alkaline soil, in which iron availability is drastically reduced. We observed that *fpn3* single mutants were smaller than wild type (Figure 5A). As an alternative approach to verify the low iron growth phenotype, we quantified the root lengths and shoot fresh weights of the *fpn3* and wild type seedlings germinated in iron sufficient medium (Figure 5B) or in medium without iron (Figure 5C). Under iron deficient conditions, *fpn3* mutant seedlings exhibited decreased shoot fresh weights (Figure

5C). The growth defect of *fpn3* on iron-deficient medium and alkaline soil consistently showed that *FPN3* is necessary for optimal growth under iron limiting conditions.

Gene expression profiles imply that iron accumulates in *fpn3* mitochondria and that *fpn3* shoots have less iron

Trafficking of iron between subcellular compartments is crucial for iron homeostasis. Thus, we predicted that expression of organellar iron homeostasis genes would be affected in *fpn3* mutant lines. Transcript levels of all vegetative ferritin genes, *FERRITIN1 (FER1)*, *FER3*, and *FER4*, were significantly affected in the shoot tissue of the *fpn3* mutant (Figure 6). Ferritins sequester iron, and the transcript levels of *FER1/3/4* are increased in the presence of iron in plants (Petit et al., 2001; Arnaud et al., 2006). It has been proposed that plant ferritins play a major role in preventing iron-induced oxidative stress in plants (Ravet et al., 2009). Transcript levels of *FER1* and *FER3*, which encode plastid-localized ferritins, were significantly lower in iron-sufficient shoots of *fpn3* compared to wild type, implying that *fpn3* shoots might contain less iron than wild type (Figure 6). On the contrary, the expression of *FER4* was approximately 2 and 2.9-fold higher in *fpn3-1* and *fpn3-2*, respectively, compared to wild type (Figure 6). *FER4* encodes a dual-targeted ferritin that localizes to mitochondria and plastids. FER4 is the only mitochondrial ferritin, as mitochondria of *fer4* cells are devoid of ferritins (Tarantino et al., 2010b). Thus, the pronounced increase in *FER4* transcripts is likely caused by *fpn3-1* and *fpn3-2* mutant plants accumulating more iron in the mitochondria and chloroplasts, and higher level of *FER4* transcripts to prevent iron-induced oxidative damage.

FRO3 encodes a mitochondrial ferric chelate reductase and has been used as a marker for iron deficiency (Mukherjee et al., 2006). *FRO3* expression was about 46% and 31% higher in iron-

deficient shoots of *fpn3-1* and *fpn3-2,* respectively, compared to wild type (Figure 6). In addition, *FRO3* expression was significantly higher in *fpn3* shoots than in wild type under iron-sufficient conditions (Figure 6). Along with the expression profiles of *FER1* and *FER3*, elevated *FRO3* expression levels indicates that *fpn3* shoots might have less cytosolic iron. Contrary to the shoots, we observed similar levels of *FRO3* transcripts in *fpn3* and wild type roots (Supplementary Figure 5). Expression of another mitochondrial ferric chelate reductase gene, *FRO8*, was ~30% higher in *fpn3* shoots under iron-sufficient conditions, and there was a 2-fold increase in *fpn3* shoots under iron-deficient conditions (Figure 6). Because *FRO8* is not regulated by iron in wild type plants (Figure 6; Mukherjee et al., 2006), the higher level of *FRO8* in *fpn3* plants is most likely caused by the dysregulation of mitochondrial iron rather than by fluctuations in cytosolic iron levels. In contrast to the mitochondrial ferric chelate reductase genes, expression of *FRO7*, which encodes the chloroplast ferric chelate reductase, was not significantly different between the *fpn3* mutants and wild type; *FRO7* transcript levels were increased in iron deficiency, but similar across all three genotypes (Figure 6).

NATURAL RESISTANCE-ASSOCIATED MACROPHAGE PROTEIN 4 (NRAMP4) encodes a vacuolar iron effluxer and is induced by low cytosolic iron (Lanquar et al., 2005). Compared to wild type, *NRAMP4* expression was significantly lower in iron-deficient roots of *fpn3* (Supplementary Figure 5), whereas its expression was higher in iron-deficient shoots of *fpn3* (Figure 6). In the shoots, this observation is in accordance with the expression profiles of *FERs* and *FRO3*, which suggests less cytosolic iron in *fpn3* shoots than in wild type shoots.

Iron content is reduced in *fpn3* mutant leaves

Gene expression analysis suggested that *FPN3* was highly expressed in shoots regardless of the iron status (Figure 3I, L), and the abundance of *FRO3* transcripts in *fpn3* shoots suggested that iron levels in the mutant shoot were lower than in wild type (Figure 6). Therefore, we tested if iron content of *fpn3* mutant leaves might be affected. We conducted bulk elemental analysis of shoot and root tissues from plants grown under iron deficient and sufficient conditions using inductively coupled plasma mass spectrometry (ICP-MS). ICP-MS results verified that iron content of *fpn3* mutant shoot tissue was significantly lower than that of wild type under both iron sufficient and deficient conditions (Figure 7A). In roots, iron content was not statistically different between wild type and *fpn3* mutants under iron sufficient conditions (Figure 7B). However, iron content was significantly lower in *fpn3* mutant roots than in wild type roots under iron deficiency (Figure 7B). We then performed synchrotron x-ray fluorescence imaging (SXRF) to examine the amount and distribution of iron in leaves of *fpn3* and wild type. The overall distribution of iron was not different among genotypes (Figure 7C). The elemental map of manganese and zinc were similar compared to wild type (Supplementary Figure 6). These results suggested that the function of FPN3 is necessary to properly maintain iron levels in the leaves regardless of iron conditions and in the roots under iron deficiency. We note that our ICP-MS data correlates with the expression profile of *FPN3* in roots and shoots under iron sufficient and deficient conditions (Figure 3L).

Mitochondria and chloroplasts of *fpn3* accumulate iron

Based on the subcellular localization of FPN3 in the mitochondria and chloroplasts (Figure 1) and our yeast results that suggested FPN3 is exporting iron from these organelles (Figure 2), we predicted that iron would accumulate in the mitochondria and chloroplasts of *fpn3*. Thus, we

isolated these organelles from *fpn3* and wild type shoots. To examine the purity of our samples, Western blots were done with the chloroplasts or mitochondrial samples using antibodies against cytosolic or organellar markers (Supplementary Figures 8, 9). We then quantified metal concentrations using ICP-MS. As predicted, chloroplasts and mitochondria from both *fpn3-1* and *fpn3-2* contained significantly more iron compared to their counterparts in wild type (Figure 8A, 8B). The accumulation of iron in *fpn3* mutant chloroplasts and mitochondria provides strong evidence that supports the role of FPN3 as a mitochondrial and chloroplast iron exporter.

***fpn3* mitochondria exhibit abnormal morphology under iron deficient conditions**

Abnormal chloroplast ultrastructure has been observed in mutants defective in iron metabolism or in plants grown under iron deficiency in multiple plant species (Bogorad et al., 1959; Stocking, 1975; Platt-Aloia et al., 1983; Duy et al., 2007; Vigani et al., 2015). In addition to chloroplasts, the ultrastructure of mitochondria has also been shown to be affected by iron deficiency in plants (Pascal and Douce, 1993; Vigani et al., 2015). Therefore, we examined the ultrastructure of chloroplasts and mitochondria in *fpn3* and wild type leaves using transmission electron microscopy (TEM). Our TEM images revealed that the mitochondrial ultrastructure of *fpn3* mitochondria was notably different from that of wild type under iron deficient conditions (Figure 9). Mitochondria of *fpn3* mutants were enlarged and the outer and inner membranes appeared deformed after grown in iron deficiency (Figure 9J-O), but such phenotypes were not detected under iron sufficient conditions (Figure 9A-I). In contrast, we did not observe differences in the chloroplast ultrastructure between wild type and *fpn3* regardless of the iron conditions tested (Figure 9A-C, G-I, J-O). Overall, the iron-dependent mitochondrial phenotype strongly suggests that FPN3 function is critical for mitochondria under iron deficient conditions.

DISCUSSION

A dual-targeted mitochondrial/chloroplast iron exporter of the FPN family

FPNs have been extensively studied in vertebrate species, in which one FPN that is localized to the plasma-membrane exports iron from the cell into the plasma (Drakesmith et al., 2015). In many plant species, multiple FPN/IREG paralogs are present and localize to different sub-cellular compartments. FPN1/IREG1 in *Arabidopsis thaliana* (Morrissey et al., 2009) and the nodule-specific FPN2 in *Medicago truncatula* (Escudero et al., 2020) are targeted to the plasma membrane, whereas the Arabidopsis FPN2/IREG2 (Schaaf et al., 2006; Morrissey et al., 2009) and buckwheat IREG (Yokosho et al., 2016) were identified on the tonoplast. Although MAR1 was reported to be targeted to the chloroplasts (Conte et al., 2009), our study shows that MAR1, or FPN3/IREG3, is dual-targeted to mitochondria and chloroplasts (Figure 1).

This study suggests that FPN3 is exporting iron from the mitochondria and chloroplasts. Our results from yeast cells expressing *FPN3* (Figure 2), expression profiles of iron homeostasis genes in *fpn3* mutants (Figure 6; Supplementary Figure 5), and the iron content of isolated chloroplasts and mitochondria (Figure 8) are all consistent with our proposed direction of iron transport by FPN3. Under the hypothesis that FPN3 is of bacterial origin, its directionality is consistent with iron export from its ancestral cytoplasm. Based on the subcellular localization of FPN3 (Figure 1) and the endosymbiotic origin of mitochondria and chloroplasts (Raven and Allen, 2003; Rockwell et al., 2014; Zimorski et al., 2014; Roger et al., 2017), it is reasonable to speculate that FPN3 diverged from a bacterial ancestor. Prokaryotic ferroportins have not been extensively studied, but a bacterial FPN from *Bdellovibrio bacteriovorus* has been reported (Bonaccorsi di Patti et al., 2015; Taniguchi et al., 2015).

The physiological role of FPN3

FPN3 was previously reported as MAR1 and proposed to opportunistically transport aminoglycoside class antibiotics (Conte et al., 2009; Conte and Lloyd, 2010). In this report, we add new information that is critical to understanding the physiological role of FPN3/MAR1. First, our results show that FPN3 is dual-targeted to the mitochondria and chloroplasts and plays a critical role in mitochondrial iron homeostasis. Conte et al (2009) reported that MAR1 was targeted to chloroplasts based on microscopy with protoplasts transiently expressing either MAR1-YFP or the predicted transit peptide of MAR1 fused with YFP and chlorophyll autofluorescence as a marker. Here, using both transient and stable expression systems, we observed that FPN3-GFP is co-localized with mitochondrial and plastid markers (Figure 1). Furthermore, we detected abnormal mitochondrial morphology in iron deficient *fpn3* mutant leaves (Figure 9). Our TEM results indicate that FPN3 plays an iron-dependent role that is crucial in the mitochondria. It is also possible that the chloroplasts may be better equipped with mechanisms that compensate for defective FPN3 function under iron deficient conditions than the mitochondria.

Second, we show that FPN3 exports iron from mitochondria and chloroplasts and most likely transports ferrous iron ions. Conte et al (2009) speculated that MAR1 may be importing the polyamine iron chelator, nicotianamine (NA), based on its structural similarity to aminoglycoside class antibiotics. However, the presence of the highly conserved iron ion binding residues in FPN3/IREG3 (Supplementary Figure 1) and the iron phenotypes of yeast cells expressing *FPN3* that are analogous to yeast cells expressing *MMT1/2* (Figure 2) rather strongly support the idea that ferrous iron ions are most likely to be transported via FPN3/IREG3. Our data further suggests that FPN3/IREG3 is exporting iron from mitochondria and chloroplasts,

based on the yeast results (Figure 2) and iron accumulation quantified by ICP-MS with isolated chloroplasts and mitochondria (Figure 8A, B). It is noteworthy that in a recent study, BnMAR1, the FPN3/IREG3 ortholog in *Brassica napus*, was speculated to be involved in iron release from the plastids based on the correlation between its gene expression and chloroplast iron content (Pham et al., 2020). We noted that the accumulation of other essential metals, such as manganese, zinc, and copper, was affected in *fpn3* chloroplasts and mitochondria (Supplementary Figure 7), which may suggest compensatory effects to accommodate for the accumulation of iron in the mutant. Further studies will be necessary to test if other metals could also be transported by FPN3.

Third, we show that *FPN3* is constitutively expressed regardless of the iron conditions in the shoots, whereas its transcript levels are increased by iron deficiency in the roots. We note that our data contradicts the results of Conte et al (2009), who reported down-regulation of *MAR1* expression in low iron conditions by RT-qPCR with whole seedlings. However, multiple transcriptomics datasets corroborate our results and show that *FPN3/IREG3* transcript level is higher in wild type roots under iron deficiency (Dinneny et al., 2008; Buckhout et al., 2009; Yang et al., 2010; Mai et al., 2016; Khan et al., 2018; Park et al., 2019) but not iron-regulated in shoots (Rodríguez-Celma et al., 2013; Khan et al., 2018).

The differential expression of *FPN3* in roots and shoots under iron-deficient or iron-sufficient conditions (Figure 3G-L) implies that FPN3 may be playing different roles in roots and shoots. Genes involved in iron acquisition or mobilization are generally induced under iron deficiency (Connolly et al., 2002; Varotto et al., 2002; Vert et al., 2002; Thomine et al., 2003; Lanquar et al., 2005), whereas steady-state transcript levels of multiple metal homeostasis genes that load iron into a subcellular organelles remain unaffected by the availability of metals in the

environment (Desbrosses-Fonrouge et al., 2005; Kim et al., 2006; Klaumann et al., 2011; Zhang et al., 2012). Our split root data revealed that the transcript level of *FPN3* in roots is regulated in response to the local availability of iron, but also indicated that systemic signals may also contribute to *FPN3* regulation (Figure 3). This suggests that FPN3 is releasing iron from chloroplasts/plastids and mitochondria in the roots when iron deficiency in the rhizosphere is sensed. We speculate that FPN3 may be releasing iron into the root cytoplasm so that it can be reallocated within the cell to help cope with iron deficiency. Alternatively, FPN3 might be releasing iron to protect iron-induced oxidative stress or to adjust metabolic needs under iron deficiency. As a response to iron deficiency, metabolic pathways in plants, including those that occur in chloroplasts and mitochondria, are coordinately remodeled in both roots and shoots (Thimm et al., 2001; López-Millán et al., 2013; Rodríguez-Celma et al., 2013). In the shoots, *FPN3* is constitutively expressed in shoots regardless of the plant iron status (Figure 3G-L) and throughout development according to transcriptomic datasets (Winter et al., 2007). Although *FPN3* does not appear to be iron-regulated at the transcriptional level in the shoots, the abnormal mitochondria morphology detected in iron deficient *fpn3* leaves suggest a critical role for FPN3 under iron deficiency (Figure 9).

Implications of a mitochondrial iron exporter

The altered ultrastructure of mitochondria in iron deficient *fpn3* indicate that FPN3 is important for mitochondrial function (Figure 9). While the mechanism behind the enlarged mitochondria of iron deficient *fpn3* remains to be understood, it is noteworthy that impaired ion homeostasis is known to affect mitochondrial volume (Szabo and Zoratti, 2014; Teardo et al., 2015). Swollen mitochondria have been observed upon anaerobic treatment, decreased metabolism, or oxidative stress (Lee et al., 2002; Vartapetian et al., 2003; Yoshinaga et al., 2005). We speculate that

oxidative stress or metabolic constraints caused by dysregulated iron homeostasis in iron deficient *fpn3* mitochondria might have resulted in the compromised mitochondrial ultrastructure.

Mitochondrial metabolism was found to be less affected than chloroplast metabolism under mild iron deficiency (Hantzis et al., 2017). However, it is noteworthy that improper FPN3 function appears to have a greater impact on the mitochondria than chloroplasts (Figure 9). The mitochondrial phenotype of *fpn3* signifies the importance of iron export from the mitochondria under iron deficient conditions. It has been well-established that chloroplasts are the most iron-rich organelle in plant cells and vacuoles serve as the major iron storage compartment, and a few studies have provided evidence that mitochondria can contribute as an additional intracellular iron reservoir. In yeast *Δccc1* mutant cells that lack the vacuolar iron importer Ccc1, overexpressing *MRS3* and *MRS4*, which encode mitochondrial iron importers of the mitoferrin family, suppressed iron toxicity (Lin et al., 2011). Furthermore, MMT1 and MMT2, which belong to the cation diffusion facilitator (CDF) family, export mitochondrial iron and overexpression of *MMT1/2* results in multiple phenotypes that support the idea that mitochondria could function as an iron storage organelle (Li et al., 2014). Studies in cucumber implied that plant mitochondria are also capable of storing iron, similar to plastids and the vacuole (Migocka et al., 2018). It was proposed that CDF transporters, CsMTP7 and CsMTP6, might work in concert to move iron into and out of the mitochondria. It is interesting to note that mitochondrial iron import mediated by mitoferrins is common across multiple organisms, such as in yeast, mammals, worm, fruit fly, rice, and Arabidopsis (Mühlenhoff et al., 2003; Shaw et al., 2006; Metzendorf et al., 2009; Paradkar et al., 2009; Bashir et al., 2011; Ren et al., 2012; Jain et al., 2019). Unlike mitochondrial iron import, we speculate mechanisms to export

mitochondrial iron are more diverse. FPNs do not exist in yeast and mitochondrial FPNs have not been found in vertebrates or invertebrates, to our knowledge. In mammalian mitochondria, a ATP-binding cassette (ABC) transporter, ABCB8, is involved in exporting iron (Ichikawa et al., 2012). The presence of a mitochondrial iron exporter is necessary, but not sufficient to suggest that mitochondria might function as a subcellular iron store. Nevertheless, our work shows that FPN3 is regulating mitochondrial iron and implies a potential role of mitochondria as an iron reservoir. The higher expression of *FER4* in *fpn3* than in wild type (Figure 6) is also consistent with the view that mitochondria could store iron. We postulate that mitochondrial ferritin may play a more dynamic function to assist iron storage in addition to protecting mitochondria from iron-induced oxidative damage.

In conclusion, our work has uncovered some of the physiological roles for FPN3 by providing evidence that FPN3 is an iron exporter dual-targeted to mitochondria and chloroplasts, and is crucial for iron homeostasis in these organelles. Further studies are necessary to elucidate the mechanisms underlying the phenotypes observed and the potential effect of FPN3 on mitochondrial and chloroplast metabolism and oxidative stress. Future work should also address potential crosstalk among chloroplasts, mitochondria, and vacuoles to comprehensively understand organellar iron trafficking and homeostasis in plant cells.

MATERIALS AND METHODS

Transient expression of FPN3-GFP in Arabidopsis protoplasts

The C-terminus of the FPN3 coding region was fused with GFP by cloning into the *Xba*I and *Bam*HI sites of the pCamV3-GFP vector, using primers 5'-tctagaatggttgtttcaatggctttggtc-3' and 5'-ggatccaatttgagagagggtcgaaggagaag-3'. The resulting construct, FPN3-GFP, was confirmed by

DNA sequencing. The pCamV3-GFP vector and F_1-ATPase-RFP were kind gifts from Inhwan Hwang. Protoplasts were isolated and co-transformed with FPN3-GFP and F_1-ATPase-RFP by the PEG method (Kim et al., 2001) and examined after 16 to 32 hours. Fluorescence images were captured with an epi-fluorescence microscope, Nikon Eclipse 80i, using the filter sets 31001 (exciter: D480/20x, dichroic: 505DCLP, emitter: D535/40m) for GFP and 31003 (exciter: D546/10x, dichroic: 560DCLP, emitter: D590/30m) for RFP. Filter sets were from Chroma Technol Corp (Rockingham, VT).

Generation of *FPN3-GFP* transgenic lines

The coding region of FPN3 was cloned from a BAC clone, F2P16 (GenBank AF007270), obtained from the Arabidopsis Biological Resource Center (ABRC) using primers 5'-caccatggttgtttcaatggctttgg-3' and 5'-atttgagagagggtcgaaggag-3' and cloned into pENTR/D-TOPO (Invitrogen). The final construct, *35Sp-FPN3-GFP*, was cloned into pGWB505 (Nakagawa et al., 2007) using Gateway LR Clonase II (Invitrogen). *35Sp-FPN3-GFP* and *35Sp-pt-RFP* were co-transformed into *Agrobacterium tumefaciens* strain LBA4404, and then into wild type Col 0 using the floral dip method (Clough and Bent, 1998). pGWB505 was a gift from Tsuyoshi Nakagawa (Addgene plasmid #74847; RRID: Addgene_74847) and *35Sp- pt-rb* (Nelson et al., 2007) was obtained from ABRC (stock #CD3-1000).

Confocal microscopy

Arabidopsis roots stably expressing *35Sp-FPN3-GFP* were imaged with the Nikon A1 Spectral Detector Confocal with FLIM Module at the Light Microscopy Core, Institute for Applied Life Science at University of Massachusetts, Amherst. Roots were stained with either MitoTracker

Red FM to label the mitochondria and z-stack images were taken with FITC and TRITC channels. Images were collected and processed with NIS-Elements software.

Yeast spot assays

For growth tests in high iron media, *pRS315-FPN3*, *pRS315-MMT1/2*, or *pRS315* vector alone was transformed into *Δccc1Δmmt1/2* or *Δmmt1/2*cells, and serial dilutions of overnight yeast cultures were spotted onto SD plates with appropriate auxotrophic supplements containing 2 mM iron (2 mM ferrous ammonium sulfate hexahydrate). The negative control plates contained media with no added iron or H_2O_2.

Aconitase assays

pRS426-FPN3 or *pRS426-MMT1/*2 with a *LEU2* marker and the *c-GDO* vector were co-transformed into Δ*ccc1* and *Δccc1 Δmmt1/2.* These transformants were inoculated in appropriate selective media (SD -Leu), grown overnight at 30ºC, and sub-cultured in 10 or 15 mL of iron-deficient media (supplemented with 80 µM BPS) or iron-sufficient media (supplemented with 250 µM $FeSO_4$) until the cells reached mid-log phase. The subcultures were harvested and washed with cold phosphate-buffered saline (PBS), and protein lysate was prepared using PBS with protease inhibitor (Pierce) via homogenization with glass beads for 10 minutes at 4ºC. Samples used in the aconitase assay were normalized with total protein concentration (Pierce Coomassie (Bradford) Assay Kit).

Generation of *FPN3p-GUS* transgenic lines and histochemical staining

A fragment containing 890 bp of upstream sequence and the *FPN3* start codon was amplified from a BAC clone, F2P16 (GenBank AF007270), obtained from the Arabidopsis Biological

Resource Center (ABRC) using primers 5'-cacccactttctcttttgttagattctagttg-3' and 5'-cattctataaat-tgattctcctcttctcc-3' and cloned into pENTR/D-TOPO (Invitrogen). The construct was cloned into pGWB533 (Nakagawa et al., 2007) using Gateway LR Clonase II (Invitrogen). The resulting *FPN3p-GUS* construct was moved into *Agrobacterium tumefaciens* strain LBA4404 and transformed into wild type Col 0 plants using the floral dip method (Clough and Bent, 1998). pGWB533 was from Tsuyoshi Nakagawa (Addgene plasmid #74872; RRID: Addgene_74872). For histochemical staining, seedlings or tissues of *FPN3p-GUS* plants were fixed and incubated with 5-bromo-4-chloro-3-indolyl β–D-glucuronide as described by (Jefferson et al., 1987). At least five seedlings from three independent T2 or T3 lines were examined, and images were obtained using the LeicaM165 FC dissecting scope and Leica LAS EZ 3.4.0 software.

Plant materials and growth conditions

Two independent alleles of *fpn3* T-DNA insertion lines, *fpn3-1* (SALK_034189) and *fpn3-2* (SALK_009286), were obtained from the Salk collection (Alonso et al., 2003). RT-qPCR verified that *FPN3* expression was drastically reduced in these lines (Supplementary Figure 3). Arabidopsis plants were grown at 22 °C under a 16/8 hour light/dark cycle in the Conviron A1000 growth chamber.

Plant growth test under iron-deficient conditions

For alkaline soil tests, seedlings were germinated and grown in normal soil (pH ~5.8), alkaline soil (pH ~8), or alkaline soil watered with soluble iron (0.5 mM Fe-EDDHA). Alkaline soil was prepared by adding approximately 1.3 g of calcium oxide per liter of soil solution (Kim et al., 2006). For growth tests on plates, seedlings were germinated vertically for 12 days on either iron-deficient media (Murashige and Skoog (MS) without iron (Caisson MSP33) supplemented

with 300 µM ferrozine) or iron-sufficient media (MS with 100 µM FeNa-EDTA (Caisson MSP34). Seedlings were photographed, and ImageJ was used to quantify root lengths. Shoots were separated and weighed on the MT5 Analytical Microbalance (Mettler Toledo).

Split root assay

For split-root samples for RT-qPCR, plants were prepared following the protocol described by Kumar et al. (2017) with slight modifications. Wild type plants were grown for 5 days on iron-sufficient medium, cut at the roots and grown for 7 days to induce split roots, and transferred to iron-deficient or iron-sufficient medium for 3 days. The plants were then washed with 0.1M citrate buffer and moved to split plates, in which one of the split roots was placed on iron-deficient medium and the other root on iron-sufficient medium. Plants were kept on split plates for 0, 6 and 12 hours before harvesting roots for RNA preparation.

Gene expression analyses

Total RNA isolated with the Agilent Plant RNA Minikit from root or shoot tissue of plants grown under iron-deficient or iron-sufficient conditions were used for gene expression analyses. The quantity and purity of RNA were examined using NanoDrop One (Thermo Scientific), and the integrity of RNA was assessed by electrophoresis using a bleach gel (Aranda et al., 2012). For RT-qPCR, first strand cDNA was synthesized from total RNA using Quanta qScript, and qPCR was conducted using BioRad SYBR Green Supermix in CFX-Connect Real-Time PCR Detection System (BioRad). The relative transcript level of genes was calculated following the ΔCt method (Schmittgen and Livak, 2008), using *ACTIN2* (*ACT2*) as an internal control. Primers were designed using QuantPrime (Arvidsson et al., 2008) and the sequences are listed in Supplementary Table 1. For Nanostring, a custom CodeSet that included probes specific to iron

homeostasis genes of interest was designed by NanoString. Gene expression analysis was conducted with the NanoString MAX/FLEX nCounter at Dartmouth College and nCounter SPRINT Profiler System at the Molecular Genetics Core Facility at Boston Children's Hospital following the manufacturer's instructions and processed using nSolver 4.0. The custom CodeSet sequences are listed in Supplementary Table 2.

Chloroplast isolation

Chloroplast isolation was conducted following Smith et al. (2003). Arabidopsis plants were grown for 4 weeks on soil. Roughly 10 g of shoot tissue was harvested, rinsed in digestion buffer (20 mM MES-KOH, pH 5.2, 400 mM sorbitol, 0.5 mM $CaCl_2$), and incubated in digestion enzyme solution (10 ml digestion buffer, 0.04 g Macerozyme R-10 (bioWORLD), 0.2 g Cellulase (bioWORLD) for 3.5 h under light. During digestion, a 40%:85% AT Percoll step gradient was prepared on ice. Upon completion of digestion, the solution was filtered through cheesecloth to harvest protoplasts. To isolate protoplasts, the filtered solution was suspended in digestion buffer and centrifuged at 100 *g* for 5 min at 4ºC, the supernatant was discarded, then the isolated protoplasts were resuspended in protoplast resuspension buffer (20 mM MES-KOH, pH 6.0, 400 mM sorbitol, 0.5 mM $CaCl_2$) before centrifuging at 100 *g* for 2 min at 4ºC and removing supernatant. Next, protoplasts were resuspended in protoplast breakage buffer (20 mM tricine-KOH, pH 8.4, 300 mM sorbitol, 5 mM EDTA, 5 mM EGTA, 10 mM $NaHCO_3$, 0.05 g BSA added per 50 mL of solution before use) and immediately filtered through a protoplast rupturing device (a syringe tube with the end cut off, with a 20 µm and 10 µm mesh, respectively, attached via electrical tape). Next, the broken chloroplasts were layered onto the 40%:85% AT Percoll step gradient and centrifuged at 2500 *g* for 10 min at 4ºC, with the brake off. A green band was visualized at the 40%85% AT Percoll interface and harvested. The

resulting solution was diluted in HEPES-sorbitol buffer, pH 8.0 (50 mM HEPES-KOH, pH 8.0, 330 mM sorbitol) and centrifuged at 700 *g* for 5 min at 4ºC. After removing the supernatant, resulting chloroplasts were resuspended in HEPES-sorbitol buffer, pH 8.0.

Chlorophyll content (chlorophyll *a* and *b*) was quantified with the NanoDrop One Spectrophotometer (ThermoFisher) following manufacturer's instructions. The following equations were used to quantify chlorophyll *a* and chlorophyll *b* content, respectively: $C_a = 14.85A^{666} - 5.14A^{650}$; $C_b = 25.48A^{650} - 7.36A^{666}$ (Porra et al., 1989; Barnes et al., 1992). Purity was confirmed via Western blots with organellar markers.

Mitochondrial isolation

Mitochondria were isolated from four-week-old Arabidopsis leaves using a protocol adapted from Keech et al., (2005). Prior to the isolation, 30mL of continuous 50% Percoll gradient (50% (v/v) Percoll, 0.3M sucrose, 10 mM TES, 1 mM EDTA, 10 mM KH_2PO_4, 1 mM glycine, pH adjusted to 7.5 with KOH) was centrifuged at 39000 *g* for 40 min and kept at 4ºC. Roughly 40-50g of tissue was homogenized in pre-chilled grinding buffer B (0.3M sucrose, 60 m TES, 2 mM EDTA, 10mM KH_2PO_4, 25 mM tetrasodium pyrophosphate, 1 mM glycine, 1% (w/v) polyvinyl-pyrrolidone-40, 1% (w/v) defatted bovine serum albumin (BSA), with 50 mM sodium ascorbate and 20 mM cysteine added and readjustment of the pH to 8.0 with KOH just prior to grinding) using a hand blender, filtered through a 20-µm nylon mesh, and centrifuged at 2500 *g* for 5 minutes to remove intact chloroplasts and thylakoid membranes. The supernatant was centrifuged at 15000 *g* for 15 minutes. The pellet obtained was resuspended in wash buffer B (0.3M sucrose, 10mM TES, 10mM KH_2PO_4, pH adjusted to 8.0 with KOH) and gently homogenized in a chilled glass homogenizer. The resuspended pellet was then layered on top of the 50% Percoll gradient and centrifuged at 15000 *g* for 20 minutes; each 30 mL density gradient

has a maximum load of mitochondria from 30g of fresh leaf tissue. After centrifugation, the mitochondria formed a whitish band near the bottom of the tube. This band was aspirated and resuspended in 0.2-0.3 mL of wash buffer B to obtain a roughly 20-fold dilution. All procedures were conducted in the cold room or at 4°C. Mitochondrial protein was quantified using DC Protein Assay (BioRad).

SXRF Imaging

The spatial distribution of iron, manganese, and zinc in hydrated leaf tissues was imaged via SXRF at the F3 station, a bending magnet beamline with multilayer monochromator, at the Cornell High Energy Synchrotron Source. Seeds were directly germinated on soil and grown at 22°C, 14 h light/10h dark photoperiod at a photo flux density of 110 µmol/m^2/sec. The nutrient solution contained the following components: 1.25 mM KNO_3, 0.625 mM KH_2PO4, 0.5 mM $MgSO_4$, 0.5 mM $Ca(NO_3)_2$, 10 µM Fe(III)HBED, 17.5 µM H_3BO_3, 3.5 µM $MnCl_2$, 0.125 µM $CuSO_4$, 0.25 µM $ZnSO_4$, 0.05 µM Na_2MoO_4, 2.5 µM NaCl, and 0.0025 µM $CoCl_2$. The hydroponic solution was changed every week. Data were analyzed and processed as described in Yan et al 2017. Briefly, the first true leaves from 22 day-old plants were detached immediately prior to imaging, placed in the wet chamber made between two layers of metal-free Kapton™ film and mounted onto 35 mm slide mounts. The 2D raster maps were acquired using a focused, monochromatic incident x-ray beam at 12.8 keV and photon flux of approximately $3x10^{10}$ photons/sec. Samples were scanned at the resolution of 30 x 30 µm and acquisition time of 0.2 sec per data point. These settings did not cause damage to plant tissues within 6-8h scans required for analysis of the full set of genotypes. Element-specific x-ray fluorescence was detected using a Vortex ME-4 Silicon Drift Detector (SDD). Calibration of XRF equipment were

done using a uniform thin metal film standard during each experiment. Data were processed with Praxes, a software that employs PyMca libraries in batch mode (Solé et al., 2007).

ICP-MS analysis

Shoot iron content of Col 0*, fpn3-1,* and *fpn3-2* was measured by ICP-MS and normalized with dry weight. Plants were grown following the same procedure as the growth test on low iron plates. Dried shoot, root, chloroplast, and mitochondrial samples of Col 0, *fpn3-1,* and *fpn3-2* were digested with nitric acid and analyzed with the Perkin-Elmer NexION 350D ICP-MS at the Mass Spectrometry Core, Institute for Applied Life Science at University of Massachusetts, Amherst. Metal content was recorded in parts per billion (ppb) and normalized to the dry mass (mg; shoot and root tissue), chlorophyll content (µg; isolated chloroplast) or total protein (µg; isolated mitochondria) of each sample. Mean values of 4 or 5 replicates are shown with SE.

Transmission electron microscopy (TEM)

Excised cotyledons of Arabidopsis seedlings treated under iron sufficient or deficient conditions were fixed by immersing them in 2.5% glutaraldehyde/ 2% paraformaldehyde in 0.1 M Na Cacodylate buffer (pH 7.2) and incubating them under vacuum for 30 min. After this primary fixation, the samples were rinsed three times in fresh fixation buffer for 10 min. each time and were secondarily fixed with 1.0% osmium tetroxide in ddH_2O (w/v) for 1hr at room temperature. The samples were then rinsed again three times in ddH_2O and then placed in 1% aqueous uranyl acetate (w/v) in the refrigerator overnight (tertiary fixation). After three more rinses in ddH_2O, the samples were then dehydrated through a graded series of ethanol (10%, 30%, 50%, 75%, 85%, 95%, and 100% for 3 changes). Infiltration was accomplished by running the samples through ethanol 100%: Spurr's resin-hard formulation (75:25 / V:V) for 1 h at room temperature,

then to ethanol 100%: Spurr's resin-hard formulation (50:50 / V:V) and finally to ethanol 100%: Spurr's resin-hard formulation (25:75 / V:V) overnight. The following day the samples were transferred through 5 changes of 100% Spurr's epoxy resin each 1 hr long, and then placed in molds and polymerized for two days at 68° C. Ultrathin sections (approx. 70 nm thick) were collected onto 200 mesh copper support grids and contrasted with Uranyl Acetate and Lead Citrate and then imaged using a CM 10 transmission electron microscope, under 100Kv accelerating voltage. Images were recorded with a Gatan Erlangshen CCD Digital camera.

ACKNOWLEDGEMENTS

We are grateful to Mary Lou Guerinot, Jerry Kaplan, and Elsbeth Walker for feedback on this manuscript. We also thank Jerry Kaplan for the yeast strains and plasmids used in this study, Liangtao Li for the yeast Western blot and help with aconitase assays, Elsbeth Walker for advice on the split root experiments, Inhwan Hwang for the pCamV3-GFP and F_1-ATPase-RFP plasmids, James Chambers for assistance with confocal microscopy, Britney Privett for assistance with NanoString, Steve Eyles for help with ICP-MS, and Lara Strittmatter and UMass Medical School Electron Microscopy Facility for assistance with TEM. We also thank Veronica Voronina, Joye Yang, and Aleks Merkovich for technical assistance at various stages of this project.

References

Altschul SF, Gish W, Miller W, Myers EW, Lipman DJ (1990) Basic local alignment search tool. J Mol Biol 215: 403–410

Aranda PS, LaJoie DM, Jorcyk CL (2012) Bleach gel: a simple agarose gel for analyzing RNA quality. Electrophoresis 33: 366–369

Arnaud N, Murgia I, Boucherez J, Briat J-F, Cellier F, Gaymard F (2006) An iron-induced nitric oxide burst precedes ubiquitin-dependent protein degradation for Arabidopsis AtFer1 ferritin gene expression. J Biol Chem 281: 23579–23588

Balk J, Schaedler TA (2014) Iron cofactor assembly in plants. Annu Rev Plant Biol 65: 125–153

Bashir K, Ishimaru Y, Shimo H, Nagasaka S, Fujimoto M, Takanashi H, Tsutsumi N, An G, Nakanishi H, Nishizawa NK (2011) The rice mitochondrial iron transporter is essential for plant growth. Nat Commun 2: 322

Bienfait HF, de Weger LA, Kramer D (1987) Control of the development of iron-efficiency reactions in potato as a response to iron deficiency is located in the roots. Plant Physiol 83: 244–247

Bogorad L, Pires G, Swift H (1959) The structure of chloroplasts in leaf tissue of iron deficient *Xanthium*. Brookhaven Symp. Biol.

Bonaccorsi di Patti MC, Polticelli F, Cece G, Cutone A, Felici F, Persichini T, Musci G (2014) A structural model of human ferroportin and of its iron binding site. FEBS J 281: 2851–2860

Bonaccorsi di Patti MC, Polticelli F, Tortosa V, Furbetta PA, Musci G (2015) A bacterial homologue of the human iron exporter ferroportin. FEBS Lett 589: 3829–3835

Briat J-F, Duc C, Ravet K, Gaymard F (2010) Ferritins and iron storage in plants. Biochim Biophys Acta 1800: 806–814

Brumbarova T, Bauer P, Ivanov R (2015) Molecular mechanisms governing Arabidopsis iron uptake. Trends Plant Sci 20: 124–133

Buckhout TJ, Yang TJW, Schmidt W (2009) Early iron-deficiency-induced transcriptional changes in Arabidopsis roots as revealed by microarray analyses. BMC Genomics 10: 147

Bughio N, Takahashi M, Yoshimura E, Nishizawa NK, Mori S (1997) Light-Dependent Iron Transport into Isolated Barley Chloroplasts. Plant and Cell Physiology 38: 101–105

Clemens S, Weber M (2016) The essential role of coumarin secretion for Fe acquisition from alkaline soil. Plant Signal Behav 11: e1114197

Clough SJ, Bent AF (1998) Floral dip: a simplified method for *Agrobacterium*-mediated transformation of *Arabidopsis thaliana*. Plant J 16: 735–743

Colombo C, Palumbo G, He J-Z, Pinton R, Cesco S (2014) Review on iron availability in soil: interaction of Fe minerals, plants, and microbes. J Soils Sediments 14: 538–548

Connolly EL, Fett JP, Guerinot ML (2002) Expression of the IRT1 metal transporter is controlled by metals at the levels of transcript and protein accumulation. Plant Cell 14: 1347–1357

Connorton JM, Balk J, Rodríguez-Celma J (2017) Iron homeostasis in plants - a brief overview. Metallomics 9: 813–823

Conte S, Stevenson D, Furner I, Lloyd A (2009) Multiple antibiotic resistance in Arabidopsis is conferred by mutations in a chloroplast-localized transport protein. Plant Physiol 151: 559–573

Conte SS, Chu HH, Rodriguez DC, Punshon T, Vasques KA, Salt DE, Walker EL (2013) Arabidopsis thaliana Yellow Stripe1-Like4 and Yellow Stripe1-Like6 localize to internal cellular membranes and are involved in metal ion homeostasis. Front Plant Sci 4: 283

Conte SS, Lloyd AM (2010) The MAR1 transporter is an opportunistic entry point for antibiotics. Plant Signal Behav 5: 49–52

Desbrosses-Fonrouge A-G, Voigt K, Schröder A, Arrivault S, Thomine S, Krämer U (2005) Arabidopsis thaliana MTP1 is a Zn transporter in the vacuolar membrane which mediates Zn detoxification and drives leaf Zn accumulation. FEBS Lett 579: 4165–4174

DiDonato RJ, Roberts LA, Sanderson T, Eisley RB, Walker EL (2004) Arabidopsis Yellow Stripe-Like2 (YSL2): a metal-regulated gene encoding a plasma membrane transporter of nicotianamine-metal complexes. Plant J 39: 403–414

Dinneny JR, Long TA, Wang JY, Jung JW, Mace D, Pointer S, Barron C, Brady SM, Schiefelbein J, Benfey PN (2008) Cell identity mediates the response of Arabidopsis roots to abiotic stress. Science 320: 942–945

Divol F, Couch D, Conéjéro G, Roschzttardtz H, Mari S, Curie C (2013) The Arabidopsis YELLOW STRIPE LIKE4 and 6 transporters control iron release from the chloroplast. Plant Cell 25: 1040–1055

Drakesmith H, Nemeth E, Ganz T (2015) Ironing out Ferroportin. Cell Metab 22: 777–787

Durrett TP, Gassmann W, Rogers EE (2007) The FRD3-mediated efflux of citrate into the root vasculature is necessary for efficient iron translocation. Plant Physiol 144: 197–205

Duy D, Stübe R, Wanner G, Philippar K (2011) The chloroplast permease PIC1 regulates plant growth and development by directing homeostasis and transport of iron. Plant Physiol 155: 1709–1722

Duy D, Wanner G, Meda AR, von Wirén N, Soll J, Philippar K (2007) PIC1, an ancient permease in Arabidopsis chloroplasts, mediates iron transport. Plant Cell 19: 986–1006

Escudero V, Abreu I, Tejada-Jiménez M, Rosa-Núñez E, Quintana J, Prieto RI, Larue C, Wen J, Villanova J, Mysore KS, et al (2020) Medicago truncatula Ferroportin2 mediates iron import into nodule symbiosomes. New Phytol. doi: 10.1111/nph.16642

Fourcroy P, Sisó-Terraza P, Sudre D, Savirón M, Reyt G, Gaymard F, Abadía A, Abadia J, Alvarez-Fernández A, Briat J-F (2014) Involvement of the ABCG37 transporter in secretion of scopoletin and derivatives by Arabidopsis roots in response to iron deficiency. New Phytol 201: 155–167

Foury F, Roganti T (2002) Deletion of the mitochondrial carrier genes MRS3 and MRS4 suppresses mitochondrial iron accumulation in a yeast frataxin-deficient strain. J Biol Chem 277: 24475–24483

García MJ, Romera FJ, Stacey MG, Stacey G, Villar E, Alcántara E, Pérez-Vicente R (2013) Shoot to root communication is necessary to control the expression of iron-acquisition genes in Strategy I plants. Planta 237: 65–75

Grusak MA, Pezeshgi S (1996) Shoot-to-Root Signal Transmission Regulates Root Fe(III) Reductase Activity in the dgl Mutant of Pea. Plant Physiol 110: 329–334

Halliwell B, Gutteridge JM (1992) Biologically relevant metal ion-dependent hydroxyl radical generation. An update. FEBS Lett 307: 108–112

Heazlewood JL, Tonti-Filippini JS, Gout AM, Day DA, Whelan J, Millar AH (2004) Experimental analysis of the Arabidopsis mitochondrial proteome highlights signaling and regulatory components, provides assessment of targeting prediction programs, and indicates plant-specific mitochondrial proteins. Plant Cell 16: 241–256

Ichikawa Y, Bayeva M, Ghanefar M, Potini V, Sun L, Mutharasan RK, Wu R, Khechaduri A, Jairaj Naik T, Ardehali H (2012) Disruption of ATP-binding cassette B8 in mice leads to cardiomyopathy through a decrease in mitochondrial iron export. Proc Natl Acad Sci USA 109: 4152–4157

Jain A, Dashner ZS, Connolly EL (2019) Mitochondrial Iron Transporters (MIT1 and MIT2) Are Essential for Iron Homeostasis and Embryogenesis in Arabidopsis thaliana. Front Plant Sci 10: 1449

Jaquinod M, Villiers F, Kieffer-Jaquinod S, Hugouvieux V, Bruley C, Garin J, Bourguignon J (2007) A Proteomics Approach Highlights a Myriad of Transporters in the Arabidopsis thaliana Vacuolar Membrane. Plant Signal Behav 2: 413–415

Le Jean M, Schikora A, Mari S, Briat J-F, Curie C (2005) A loss-of-function mutation in AtYSL1 reveals its role in iron and nicotianamine seed loading. Plant J 44: 769–782

Jefferson RA, Kavanagh TA, Bevan MW (1987) GUS fusions: beta-glucuronidase as a sensitive and versatile gene fusion marker in higher plants. EMBO J 6: 3901–3907

Jeong J, Cohu C, Kerkeb L, Pilon M, Connolly EL, Guerinot ML (2008) Chloroplast Fe(III) chelate reductase activity is essential for seedling viability under iron limiting conditions. Proc Natl Acad Sci USA 105: 10619–10624

Jeong J, Connolly EL (2009) Iron uptake mechanisms in plants: Functions of the FRO family of ferric reductases. Plant Sci 176: 709–714

Jeong J, Merkovich A, Clyne M, Connolly EL (2017) Directing iron transport in dicots: regulation of iron acquisition and translocation. Curr Opin Plant Biol 39: 106–113

Jin JB, Bae H, Kim SJ, Jin YH, Goh C-H, Kim DH, Lee YJ, Tse YC, Jiang L, Hwang I (2003) The Arabidopsis dynamin-like proteins ADL1C and ADL1E play a critical role in mitochondrial morphogenesis. Plant Cell 15: 2357–2369

Khan MA, Castro-Guerrero NA, McInturf SA, Nguyen NT, Dame AN, Wang J, Bindbeutel RK, Joshi T, Jurisson SS, Nusinow DA, et al (2018) Changes in iron availability in Arabidopsis are rapidly sensed in the leaf vasculature and impaired sensing leads to opposite transcriptional programs in leaves and roots. Plant Cell Environ 41: 2263–2276

Kim DH, Eu YJ, Yoo CM, Kim YW, Pih KT, Jin JB, Kim SJ, Stenmark H, Hwang I (2001) Trafficking of phosphatidylinositol 3-phosphate from the trans-Golgi network to the lumen of the central vacuole in plant cells. Plant Cell 13: 287–301

Kim SA, Punshon T, Lanzirotti A, Li L, Alonso JM, Ecker JR, Kaplan J, Guerinot ML (2006) Localization of iron in Arabidopsis seed requires the vacuolar membrane transporter VIT1. Science 314: 1295–1298

Klaumann S, Nickolaus SD, Fürst SH, Starck S, Schneider S, Ekkehard Neuhaus H, Trentmann O (2011) The tonoplast copper transporter COPT5 acts as an exporter and is required for interorgan allocation of copper in Arabidopsis thaliana. New Phytol 192: 393–404

Kobayashi T, Nozoye T, Nishizawa NK (2018) Iron transport and its regulation in plants. Free Radic Biol Med 133: 11–20

Kumar RK, Chu H-H, Abundis C, Vasques K, Rodriguez DC, Chia J-C, Huang R, Vatamaniuk OK, Walker EL (2017) Iron-Nicotianamine Transporters Are Required for Proper Long Distance Iron Signaling. Plant Physiol 175: 1254–1268

Lanquar V, Lelièvre F, Bolte S, Hamès C, Alcon C, Neumann D, Vansuyt G, Curie C, Schröder A, Krämer U, et al (2005) Mobilization of vacuolar iron by AtNRAMP3

and AtNRAMP4 is essential for seed germination on low iron. EMBO J 24: 4041–4051

Li L, Miao R, Bertram S, Jia X, Ward DM, Kaplan J (2012) A role for iron-sulfur clusters in the regulation of transcription factor Yap5-dependent high iron transcriptional responses in yeast. J Biol Chem 287: 35709–35721

Li L, Miao R, Jia X, Ward DM, Kaplan J (2014) Expression of the yeast cation diffusion facilitators Mmt1 and Mmt2 affects mitochondrial and cellular iron homeostasis: evidence for mitochondrial iron export. J Biol Chem 289: 17132–17141

Lin H, Li L, Jia X, Ward DM, Kaplan J (2011) Genetic and biochemical analysis of high iron toxicity in yeast: iron toxicity is due to the accumulation of cytosolic iron and occurs under both aerobic and anaerobic conditions. J Biol Chem 286: 3851–3862

Mai H-J, Pateyron S, Bauer P (2016) Iron homeostasis in Arabidopsis thaliana: transcriptomic analyses reveal novel FIT-regulated genes, iron deficiency marker genes and functional gene networks. BMC Plant Biol 16: 211

Marschner P, ed (2012) Marschner's Mineral Nutrition of Higher Plants, 3rd ed.

Mendoza-Cózatl DG, Xie Q, Akmakjian GZ, Jobe TO, Patel A, Stacey MG, Song L, Demoin DW, Jurisson SS, Stacey G, et al (2014) OPT3 is a component of the iron-signaling network between leaves and roots and misregulation of OPT3 leads to an over-accumulation of cadmium in seeds. Mol Plant 7: 1455–1469

Metzendorf C, Wu W, Lind MI (2009) Overexpression of Drosophila mitoferrin in l(2)mbn cells results in dysregulation of Fer1HCH expression. Biochem J 421: 463–471

Migocka M, Małas K, Maciaszczyk-Dziubinska E, Papierniak A, Posyniak E, Garbiec A (2018) Cucumber metal tolerance protein 7 (CsMTP7) is involved in the accumulation of Fe in mitochondria under Fe excess. Plant J 95: 988–1003

Morrissey J, Baxter IR, Lee J, Li L, Lahner B, Grotz N, Kaplan J, Salt DE, Guerinot ML (2009) The ferroportin metal efflux proteins function in iron and cobalt homeostasis in Arabidopsis. Plant Cell 21: 3326–3338

Mühlenhoff U, Stadler JA, Richhardt N, Seubert A, Eickhorst T, Schweyen RJ, Lill R, Wiesenberger G (2003) A specific role of the yeast mitochondrial carriers MRS3/4p in mitochondrial iron acquisition under iron-limiting conditions. J Biol Chem 278: 40612–40620

Mukherjee I, Campbell NH, Ash JS, Connolly EL (2006) Expression profiling of the Arabidopsis ferric chelate reductase (FRO) gene family reveals differential regulation by iron and copper. Planta 223: 1178–1190

Müller B, Kovács K, Pham H-D, Kavak Y, Pechoušek J, Machala L, Zbořil R, Szenthe K, Abadía J, Fodor F, et al (2019) Chloroplasts preferentially take up ferric-citrate over iron-nicotianamine complexes in Brassica napus. Planta 249: 751–763

Nakagawa T, Suzuki T, Murata S, Nakamura S, Hino T, Maeo K, Tabata R, Kawai T, Tanaka K, Niwa Y, et al (2007) Improved Gateway binary vectors: high-performance vectors for creation of fusion constructs in transgenic analysis of plants. Biosci Biotechnol Biochem 71: 2095–2100

Nelson BK, Cai X, Nebenführ A (2007) A multicolored set of in vivo organelle markers for co-localization studies in Arabidopsis and other plants. Plant J 51: 1126–1136

Paradkar PN, Zumbrennen KB, Paw BH, Ward DM, Kaplan J (2009) Regulation of mitochondrial iron import through differential turnover of mitoferrin 1 and mitoferrin 2. Mol Cell Biol 29: 1007–1016

Park EY, Tsuyuki KM, Hu F, Lee J, Jeong J (2019) PRC2-Mediated H3K27me3 Contributes to Transcriptional Regulation of FIT-Dependent Iron Deficiency Response. Front Plant Sci 10: 627

Pascal N, Douce R (1993) Effect of Iron Deficiency on the Respiration of Sycamore (Acer pseudoplatanus L.) Cells. Plant Physiol 103: 1329–1338

Petit JM, Briat JF, Lobréaux S (2001) Structure and differential expression of the four members of the Arabidopsis thaliana ferritin gene family. Biochem J 359: 575–582

Platt-Aloia KA, Thomson WW, Terry N (1983) Changes in plastid ultrastructure during iron nutrition-mediated chloroplast development. Protoplasma 114-114: 85–92

Ravet K, Touraine B, Boucherez J, Briat J-F, Gaymard F, Cellier F (2009) Ferritins control interaction between iron homeostasis and oxidative stress in Arabidopsis. Plant J 57: 400–412

Regev-Rudzki N, Karniely S, Ben-Haim NN, Pines O (2005) Yeast aconitase in two locations and two metabolic pathways: seeing small amounts is believing. Mol Biol Cell 16: 4163–4171

Ren Y, Yang S, Tan G, Ye W, Liu D, Qian X, Ding Z, Zhong Y, Zhang J, Jiang D, et al (2012) Reduction of mitoferrin results in abnormal development and extended lifespan in Caenorhabditis elegans. PLoS One 7: e29666

Robinson NJ, Procter CM, Connolly EL, Guerinot ML (1999) A ferric-chelate reductase for iron uptake from soils. Nature 397: 694–697

Roger AJ, Muñoz-Gómez SA, Kamikawa R (2017) The origin and diversification of mitochondria. Curr Biol 27: R1177–R1192

Santi S, Schmidt W (2009) Dissecting iron deficiency-induced proton extrusion in Arabidopsis roots. New Phytol 183: 1072–1084

Schaaf G, Honsbein A, Meda AR, Kirchner S, Wipf D, von Wirén N (2006) AtIREG2 encodes a tonoplast transport protein involved in iron-dependent nickel detoxification in Arabidopsis thaliana roots. J Biol Chem 281: 25532–25540

Schaaf G, Schikora A, Häberle J, Vert G, Ludewig U, Briat J-F, Curie C, von Wirén N (2005) A putative function for the arabidopsis Fe-Phytosiderophore transporter homolog AtYSL2 in Fe and Zn homeostasis. Plant Cell Physiol 46: 762–774

Schmid M, Davison TS, Henz SR, Pape UJ, Demar M, Vingron M, Schölkopf B, Weigel D, Lohmann JU (2005) A gene expression map of Arabidopsis thaliana development. Nat Genet 37: 501–506

Schmidt H, Günther C, Weber M, Spörlein C, Loscher S, Böttcher C, Schobert R, Clemens S (2014) Metabolome analysis of *Arabidopsis thaliana* roots identifies a key metabolic pathway for iron acquisition. PLoS One 9: e102444

Schmittgen TD, Livak KJ (2008) Analyzing real-time PCR data by the comparative CT method. Nat Protoc 3: 1101–1108

Shaw GC, Cope JJ, Li L, Corson K, Hersey C, Ackermann GE, Gwynn B, Lambert AJ, Wingert RA, Traver D, et al (2006) Mitoferrin is essential for erythroid iron assimilation. Nature 440: 96–100

Shcolnick S, Keren N (2006) Metal homeostasis in cyanobacteria and chloroplasts. Balancing benefits and risks to the photosynthetic apparatus. Plant Physiol 141: 805–810

Shingles R, North M, McCarty RE (2002) Ferrous ion transport across chloroplast inner envelope membranes. Plant Physiol 128: 1022–1030

Smith MD, Schnell DJ, Fitzpatrick L, Keegstra K (2003) In vitro analysis of chloroplast protein import. Curr Protoc Cell Biol Chapter 11: Unit11.16

Solti A, Kovács K, Basa B, Vértes A, Sárvári E, Fodor F (2012) Uptake and incorporation of iron in sugar beet chloroplasts. Plant Physiol Biochem 52: 91–97

Stocking CR (1975) Iron Deficiency and the Structure and Physiology of Maize Chloroplasts. Plant Physiol 55: 626–631

Tan Y-F, O'Toole N, Taylor NL, Millar AH (2010) Divalent metal ions in plant mitochondria and their role in interactions with proteins and oxidative stress-induced damage to respiratory function. Plant Physiol 152: 747–761

Taniguchi R, Kato HE, Font J, Deshpande CN, Wada M, Ito K, Ishitani R, Jormakka M, Nureki O (2015) Outward- and inward-facing structures of a putative bacterial transition-metal transporter with homology to ferroportin. Nat Commun 6: 8545

Tarantino D, Casagrande F, Soave C, Murgia I (2010a) Knocking out of the mitochondrial AtFer4 ferritin does not alter response of Arabidopsis plants to abiotic stresses. J Plant Physiol 167: 453–460

Tarantino D, Morandini P, Ramirez L, Soave C, Murgia I (2011) Identification of an Arabidopsis mitoferrinlike carrier protein involved in Fe metabolism. Plant Physiol Biochem 49: 520–529

Tarantino D, Santo N, Morandini P, Casagrande F, Braun H-P, Heinemeyer J, Vigani G, Soave C, Murgia I (2010b) AtFer4 ferritin is a determinant of iron homeostasis in Arabidopsis thaliana heterotrophic cells. J Plant Physiol 167: 1598–1605

Terry N, Low G (1982) Leaf chlorophyll content and its relation to the intracellular localization of iron. J Plant Nutr 5: 301–310

Thomine S, Lelièvre F, Debarbieux E, Schroeder JI, Barbier-Brygoo H (2003) AtNRAMP3, a multispecific vacuolar metal transporter involved in plant responses to iron deficiency. Plant J 34: 685–695

Varotto C, Maiwald D, Pesaresi P, Jahns P, Salamini F, Leister D (2002) The metal ion transporter IRT1 is necessary for iron homeostasis and efficient photosynthesis in *Arabidopsis thaliana*. Plant J 31: 589–599

Vasconcelos MW, Gruissem W, Bhullar NK (2017) Iron biofortification in the 21st century: setting realistic targets, overcoming obstacles, and new strategies for healthy nutrition. Curr Opin Biotechnol 44: 8–15

Versaw WK, Harrison MJ (2002) A chloroplast phosphate transporter, PHT2;1, influences allocation of phosphate within the plant and phosphate-starvation responses. Plant Cell 14: 1751–1766

Vert G, Grotz N, Dédaldéchamp F, Gaymard F, Guerinot ML, Briat J-F, Curie C (2002) IRT1, an Arabidopsis transporter essential for iron uptake from the soil and for plant growth. Plant Cell 14: 1223–1233

Vert GA, Briat J-F, Curie C (2003) Dual regulation of the Arabidopsis high-affinity root iron uptake system by local and long-distance signals. Plant Physiol 132: 796–804

Vigani G, Faoro F, Ferretti AM, Cantele F, Maffi D, Marelli M, Maver M, Murgia I, Zocchi G (2015) Three-Dimensional Reconstruction, by TEM Tomography, of the Ultrastructural Modifications Occurring in Cucumis sativus L. Mitochondria under Fe Deficiency. PLoS One 10: e0129141

Waters BM, Chu H-H, Didonato RJ, Roberts LA, Eisley RB, Lahner B, Salt DE, Walker EL (2006) Mutations in Arabidopsis yellow stripe-like1 and yellow stripe-like3 reveal their roles in metal ion homeostasis and loading of metal ions in seeds. Plant Physiol 141: 1446–1458

Winter D, Vinegar B, Nahal H, Ammar R, Wilson GV, Provart NJ (2007) An "Electronic Fluorescent Pictograph" browser for exploring and analyzing large-scale biological data sets. PLoS One 2: e718

Yang TJW, Lin W-D, Schmidt W (2010) Transcriptional profiling of the Arabidopsis iron deficiency response reveals conserved transition metal homeostasis networks. Plant Physiol 152: 2130–2141

Yokosho K, Yamaji N, Mitani-Ueno N, Shen RF, Ma JF (2016) An Aluminum-Inducible IREG Gene is Required for Internal Detoxification of Aluminum in Buckwheat. Plant Cell Physiol 57: 1169–1178

Zancani M, Peresson C, Biroccio A, Federici G, Urbani A, Murgia I, Soave C, Micali F, Vianello A, Macrì F (2004) Evidence for the presence of ferritin in plant mitochondria. Eur J Biochem 271: 3657–3664

Zhai Z, Gayomba SR, Jung H-I, Vimalakumari NK, Piñeros M, Craft E, Rutzke MA, Danku J, Lahner B, Punshon T, et al (2014) OPT3 Is a Phloem-Specific Iron Transporter That Is Essential for Systemic Iron Signaling and Redistribution of Iron and Cadmium in Arabidopsis. Plant Cell 26: 2249–2264

Zhang X-Y, Zhang X, Zhang Q, Pan X-X, Yan L-C, Ma X-J, Zhao W-Z, Qi X-T, Yin L-P (2017) Zea mays Fe deficiency-related 4 (ZmFDR4) functions as an iron transporter in the plastids of monocots. Plant J 90: 147–163

Zhang Y, Xu Y-H, Yi H-Y, Gong J-M (2012) Vacuolar membrane transporters OsVIT1 and OsVIT2 modulate iron translocation between flag leaves and seeds in rice. Plant J 72: 400–410

Zimmermann P, Hirsch-Hoffmann M, Hennig L, Gruissem W (2004) GENEVESTIGATOR. Arabidopsis microarray database and analysis toolbox. Plant Physiol 136: 2621–2632

Zimorski V, Ku C, Martin WF, Gould SB (2014) Endosymbiotic theory for organelle origins. Curr Opin Microbiol 22: 38–48

FIGURE LEGENDS

Figure 1. Subcellular localization of FPN3-GFP in Arabidopsis protoplasts and stable transgenic roots. (A) Bright field image of an Arabidopsis mesophyll protoplast co-transformed with *FPN3-GFP* and a mitochondrial marker, *F_1-ATPase-RFP*. (B) Expression of FPN3-GFP. (C) Expression of F_1-ATPase-RFP. (D) Overlay image of (B) and (C) shows the co-localization of FPN3-GFP with the mitochondrial marker. Arrows in (A) and (B) indicate chloroplasts and arrowheads in (B-D) indicate co-localization of FPN3-GFP and F_1-ATPase-RFP. Scale bar in (A-D) = 5 µm. (E-F) Confocal image of an optical section of Arabidopsis root stably expressing *FPN3-GFP* (E) and stained with MitoTracker Red (F). (G) Overlay image of (E) and (F) shows the co-localization of FPN3-GFP with MitoTracker Red. Scale bar in (E-G) = 25 µm. (H-J) Confocal image of an optical section of Arabidopsis root stably co-expressing *FPN3-GFP* (H) and *pt-RFP* (I). (J) Overlay image of (H) and (I) shows the co-localization of FPN3-GFP with MitoTracker Red. Scale bar in (H-I) = 25 µm.

Figure 2. Heterologous expression of *FPN3* in yeast. (A) Spot assays in high iron media with *Δccct1Δmmt1/2* cells expressing *FPN3* or *MMT1/2*. Wild type (DY150) and *Δmmt1/2* cells transformed with an empty vector, *pRS315,* were used as controls. (B) Aconitase activity (nmol/mg protein/min) of wild type cells expressing *FPN3* or *MMT1/2* was normalized to the activity of wild type with empty vector, *pRS426* (n=5; Error bars = SE). (C) cGDO activity of wild type cells expressing *FPN3*, *MMT1/2,* or the empty vector, *pRS315.* Significant differences were determined by one-way ANOVA followed by Dunnet's test (*: $p<0.05$; n=3; Error bars = SE).

Figure 3. *FPN3* expression detected by *FPN3p-GUS* and RT-qPCR. (A-C) Histochemical staining of *FPN3p-GUS* seedlings germinated under iron sufficient conditions on day 3 (A) and day 5 (C), and a close-up image of the root tip of a day 3 seedling (B; boxed region in A). (D) *FPN3p-GUS* expression in the first true leaf of a 3-week old plant. (E, F) *FPN3p-GUS* staining in floral organs (E) and the silique (F). (G, H) *FPN3p-GUS* staining in 1-day-old imbibing seedlings germinated on iron deficient (G) or sufficient (H) media. (I) *FPN3p-GUS* staining in 3-day-old seedlings germinated on iron deficient (-Fe) or sufficient (+Fe) media. (J, K) Close-up view of iron sufficient root (J) and iron deficient root (K). Representative images of seedlings or organs from at least 6 individuals are shown. (L) Relative expression of *FPN3* in shoots and roots of wild type plants treated under iron deficient or sufficient conditions. *FPN3* transcript level was quantified by RT-qPCR and normalized with *ACT2.* (t-test; *: $p<0.05$; n=3; error bars = SE).

Figure 4. Steady state *FPN3* transcript levels in split-roots. (A) Schematic overview of iron growth conditions prior to RNA extraction. (B) *FPN3* transcript levels in split roots. Seedlings were grown under iron-deficient (-Fe) or iron-sufficient (+Fe) conditions, then each root was treated appropriately with iron-deficient or iron-sufficient media for 0, 6, or 12 hours. The iron growth conditions of each split root are denoted as: +Fe/+Fe for growth in iron sufficient conditions followed by iron sufficiency treatment; +Fe/-Fe for growth in iron sufficient conditions followed by iron deficiency treatment; -Fe/+Fe for growth in iron deficient conditions followed by iron sufficiency treatment; -Fe/-Fe for growth in iron deficient conditions followed by iron deficiency treatment. Significant differences compared to 0 hour were determined by one-way ANOVA followed by Dunnett's test (*: $p<0.05$; **: $p<0.01$; n=5; error bars = SE).

Figure 5. Growth of *fpn3* under iron deficient conditions. (A) Wild type (Col 0) and *fpn3* single mutants germinated and grown in control soil or alkaline soil (~pH 8) with or without iron irrigation. (B, C) Quantified shoot fresh weights and root lengths of wild type (Col 0), *fpn3* single mutants, germinated and grown in iron-deficient media (B; no added iron with 0.3 mM ferrozine) or iron-sufficient media (C; 100 μM Fe). We quantified the root lengths and shoot fresh weights of the *fpn3* and wild type seedlings germinated in iron sufficient media (Figure 5B) or without iron (Figure 5C). Mean values of at least 19 individuals are shown. Statistically significant differences compared to Col 0 are denoted (One-way ANOVA; Dunnett's test; *: $p < 0.05$; error bars = SE).

Figure 6. Expression of organellar iron homeostasis genes in *fpn3* shoots. Normalized steady-state level transcripts detected by NanoString. Seedlings were grown in B5 without sucrose for 2 weeks and transferred to iron-deficient or iron-sufficient media for 3 days. Mean values of normalized transcript levels are shown. Significant differences compared to Col 0 samples from the same treatment are denoted (One-way ANOVA; Dunnett's test; *: $p<0.05$; n=4; Error bars = SE).

Figure 7. Elemental analysis of *fpn3* shoots and roots (A) Iron content of shoot tissue from plants grown under iron sufficient (+Fe) and deficient (-Fe) conditions measured by ICP-MS. (B) Iron content of root tissue from plants grown under iron sufficient (+Fe) and deficient (-Fe) conditions measured by ICP-MS. Mean values of pooled quadruplicate ICP-MS samples are shown with error bars (SE). Significant differences compared to Col 0 are denoted (One-way ANOVA; Dunnett's test; *: $p<0.05$; **: $p<0.01$). (C) Synchrotron x-ray fluorescence microscopy images of iron distribution in leaves of wild type (Col 0) and *fpn3* leaves. The first true leaves of

22-day old plants grown in iron sufficient conditions were imaged at a resolution of 30 x 30 µm with 0.2 sec dwell time. Representative images of leaves from three individuals are shown. Scale bars = 1 mm.

Figure 8. Elemental analysis of chloroplasts and mitochondria isolated from *fpn3*.

(A) Iron content of chloroplasts measured by ICP-MS and normalized with chlorophyll content. (B) Iron content of mitochondria normalized with mitochondrial protein. Mean values of quadruplicate chloroplast samples and triplicate mitochondrial samples are shown with error bars (SE). Significant differences compared to the wild type, Col 0, are denoted (One-way ANOVA followed by Dunett's test; *: $p<0.05$).

Figure 9. Mitochondria and chloroplast ultrastructure of *fpn3*.

(A-I) TEM images of the wild type, Col 0 (A, D, G), *fpn3-1* (B, E, H), and *fpn3-2* (C, F, I) leaf sections from iron sufficient conditions. (D-F) Close-up images of mitochondria in wild type (D), *fpn3-1* (E), and *fpn3-2* (F). (G-I) Close-up images of thylakoids in wild type (G) and *fpn3-1* (H), and *fpn3-2* (I). (J-O) TEM images of iron deficient wild type (J, M), *fpn3-1* (K, N), and *fpn3-2* (L, O) leaf sections. Chloroplasts (c) and mitochondria (m) are labeled in the images. Scale bar = 200 nm.

Figure 1.

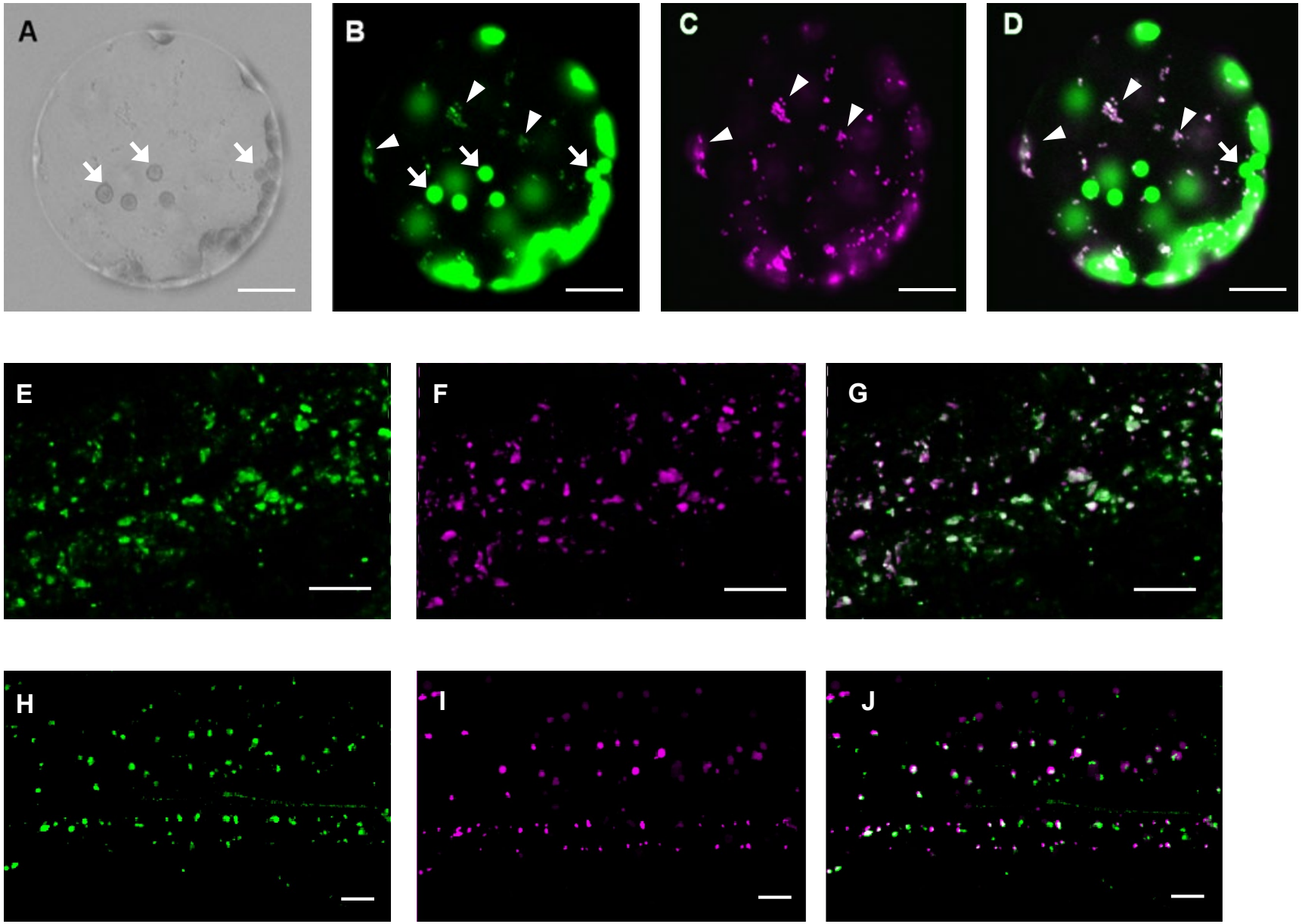

Figure 2.

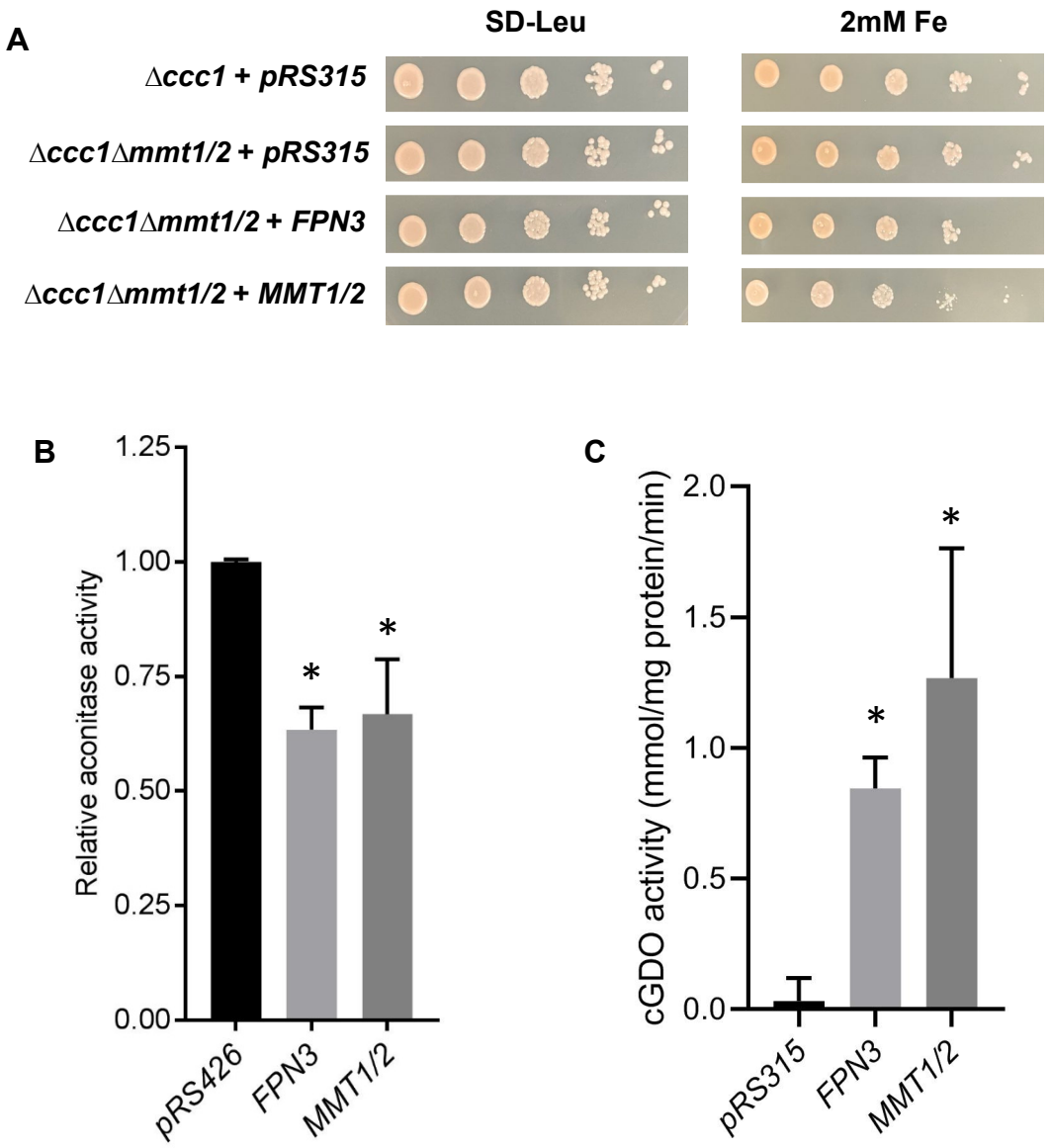
A
SD-Leu
2mM Fe
Δccc1 + pRS315
Δccc1Δmmt1/2 + pRS315
Δccc1Δmmt1/2 + FPN3
Δccc1Δmmt1/2 + MMT1/2
B
Relative aconitase activity
1.25
1.00
0.75
0.50
0.25
0.00
*
*
pRS426
FPN3
MMT1/2
C
cGDO activity (mmol/mg protein/min)
2.0
1.5
1.0
0.5
0.0
*
*
pRS315
FPN3
MMT1/2

Figure 3.

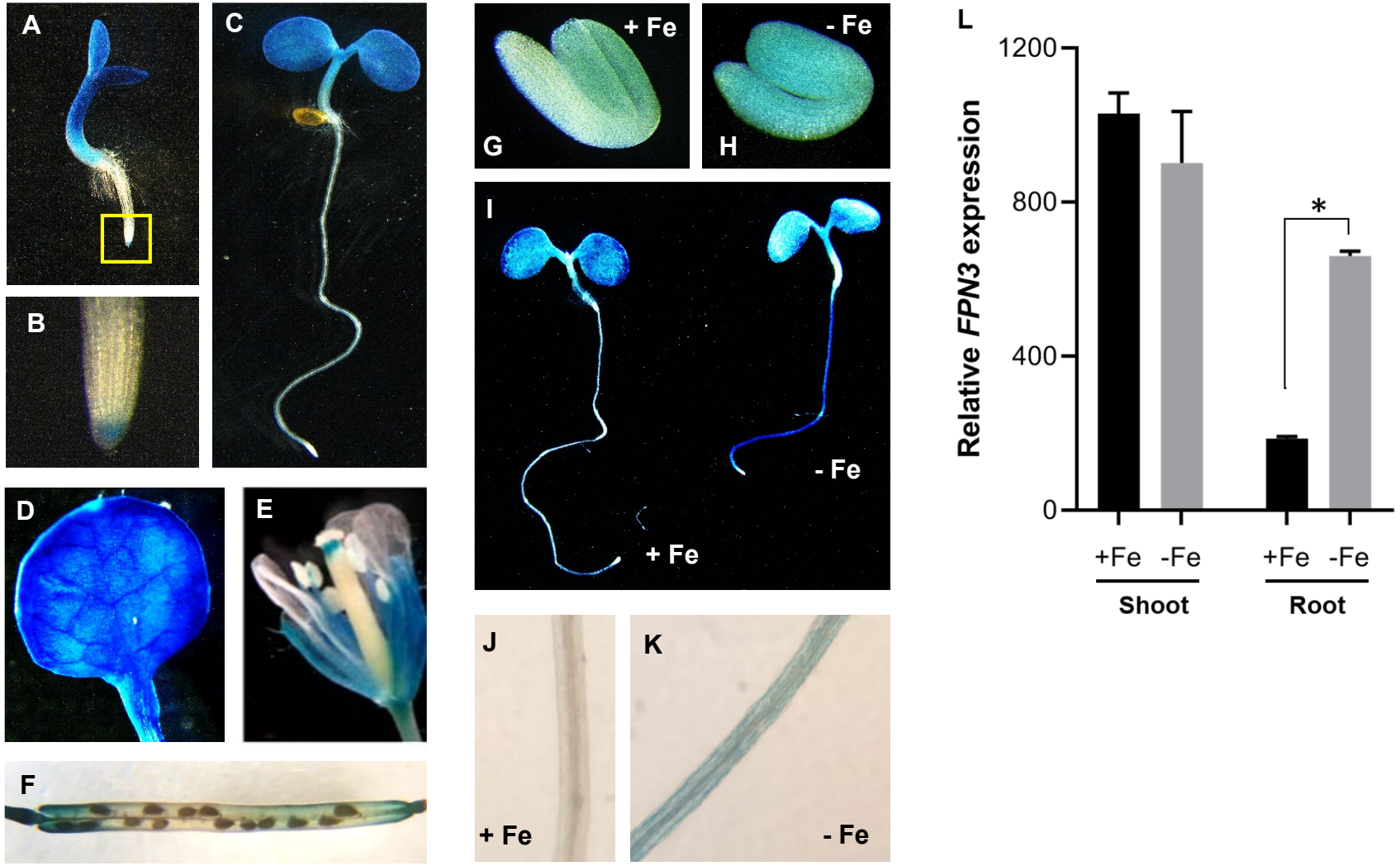
A
B
C
D
E
F
G
+ Fe
H
- Fe
I
+ Fe
- Fe
J
+ Fe
K
- Fe
L
Relative FPN3 expression
1200
800
400
0
*
+Fe
-Fe
+Fe
-Fe
Shoot
Root

Figure 4.

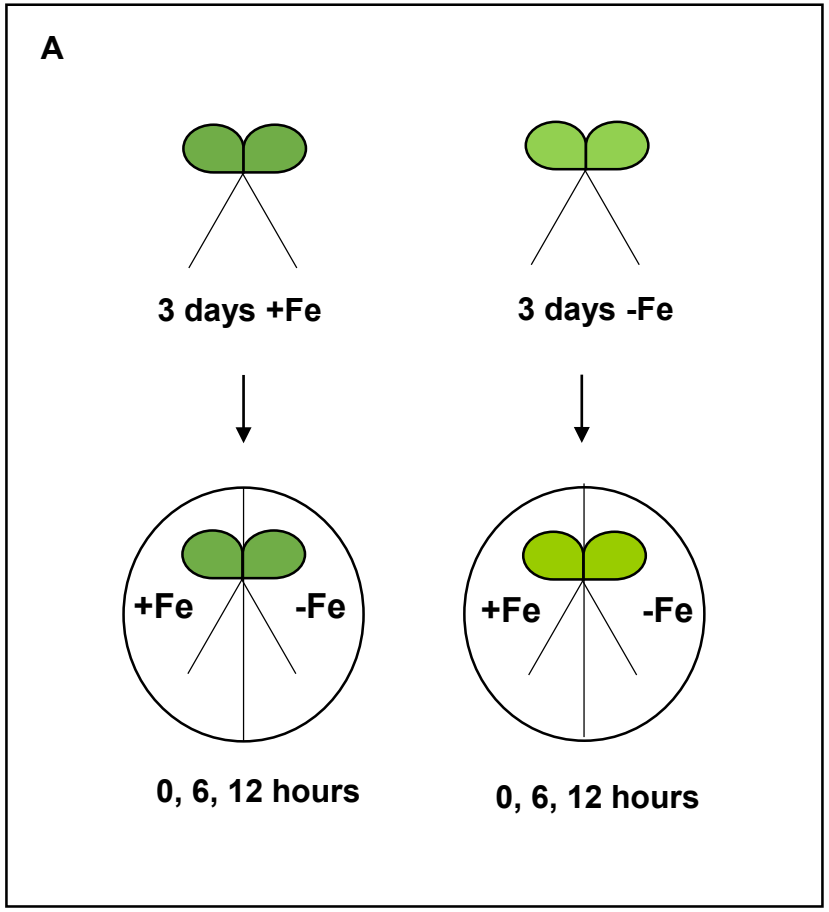
A
3 days +Fe
3 days -Fe
+Fe
-Fe
+Fe
-Fe
0, 6, 12 hours
0, 6, 12 hours

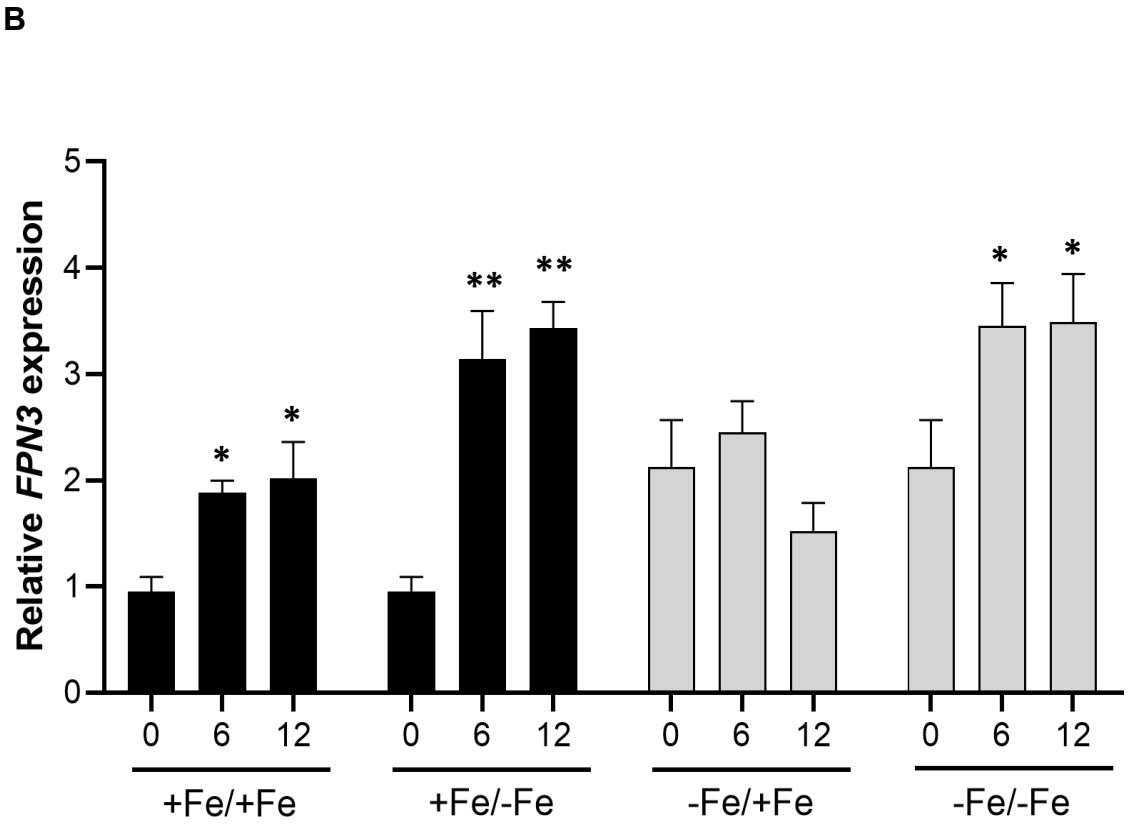
B
Relative FPN3 expression
0
1
2
3
4
5
*
*
**
**
*
*
0
6
12
0
6
12
0
6
12
0
6
12
+Fe/+Fe
+Fe/-Fe
-Fe/+Fe
-Fe/-Fe

Figure 5.

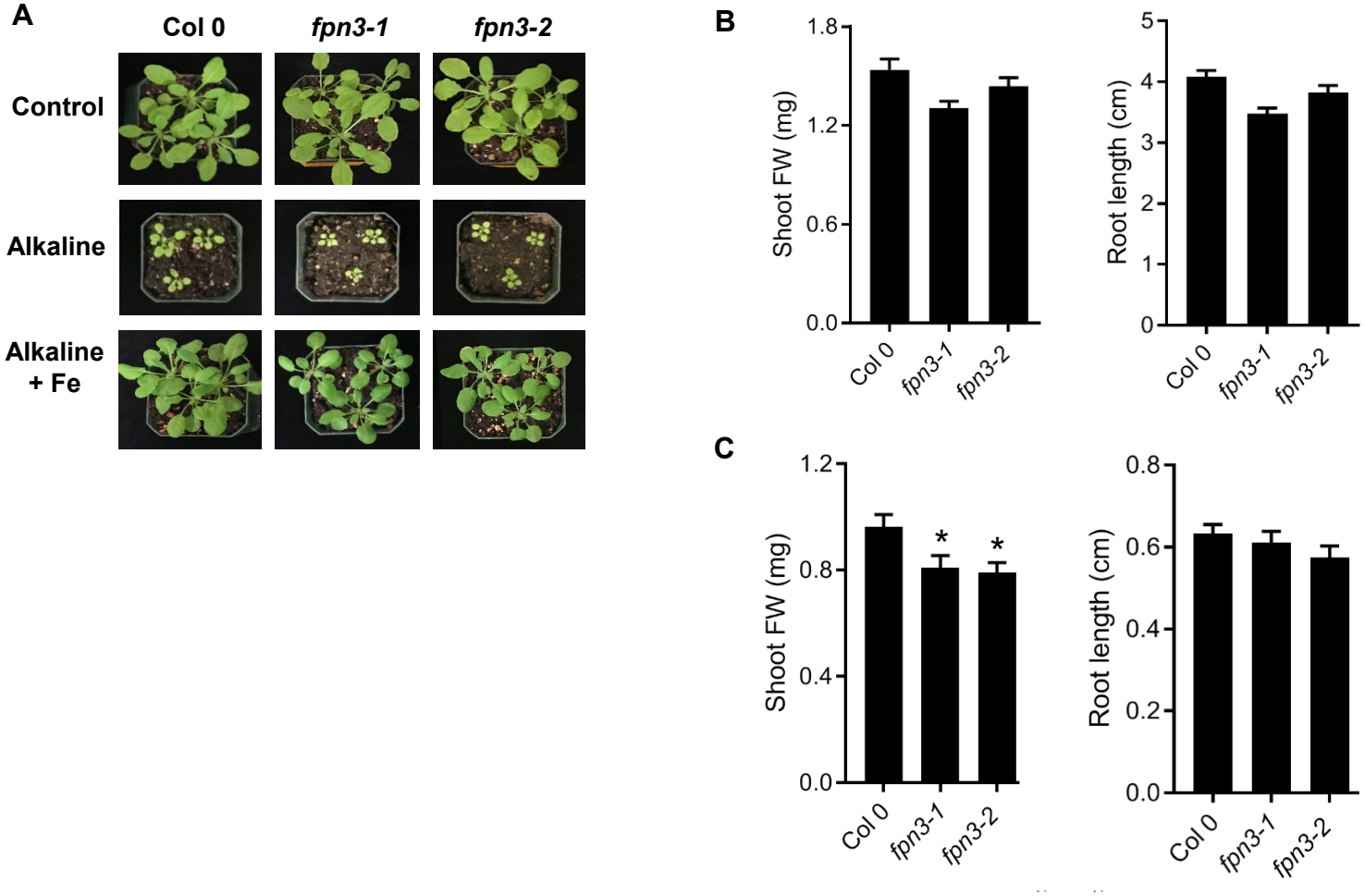
A
Col 0
fpn3-1
fpn3-2
Control
Alkaline
Alkaline + Fe
B
Shoot FW (mg)
1.8
1.2
0.6
0.0
Root length (cm)
5
4
3
2
1
0
Col 0
fpn3-1
fpn3-2
C
Shoot FW (mg)
1.2
0.8
0.4
0.0
*
*
Root length (cm)
0.8
0.6
0.4
0.2
0.0
Col 0
fpn3-1
fpn3-2

Figure 6.

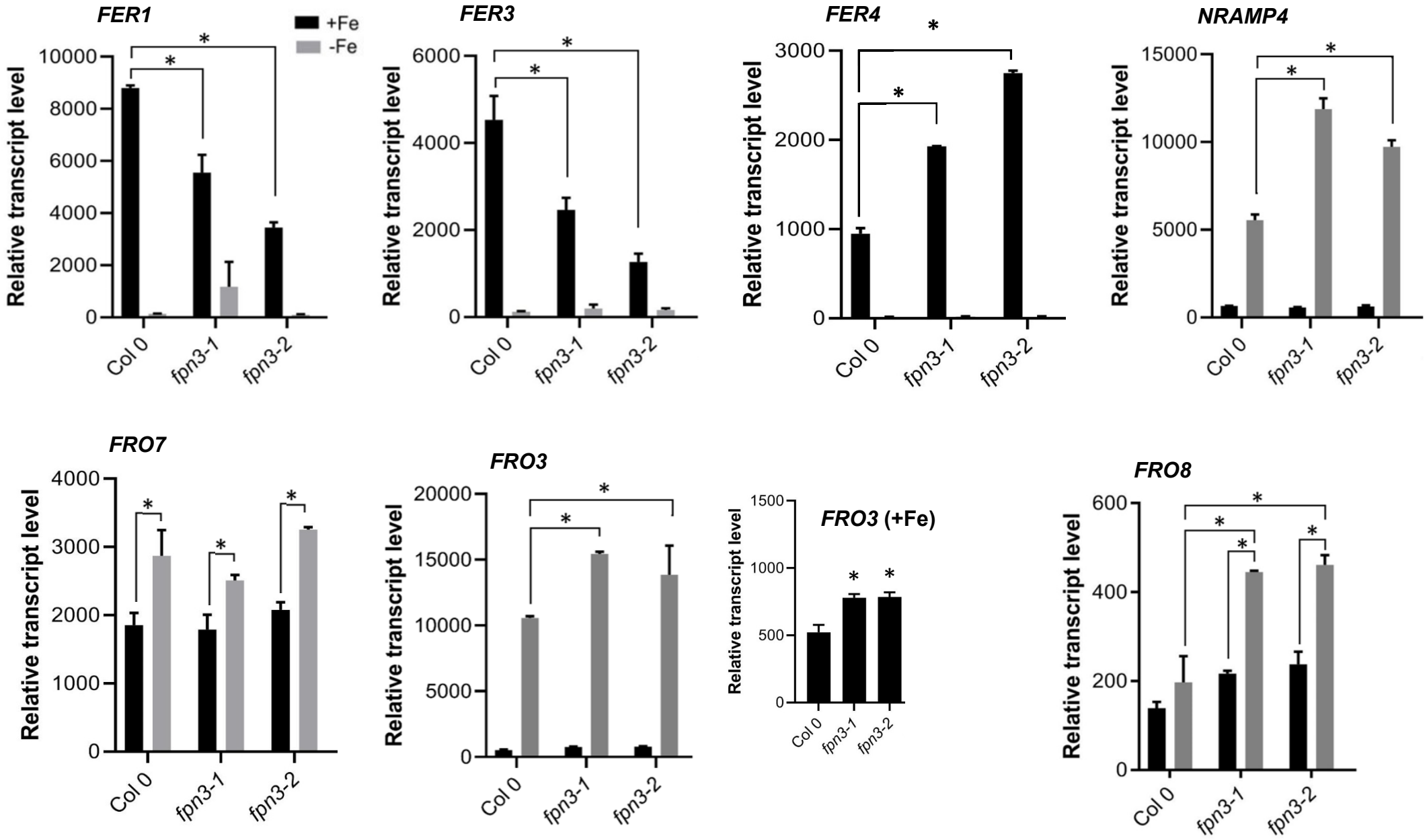
FER1
+Fe
-Fe
Relative transcript level
10000
8000
6000
4000
2000
0
Col 0
fpn3-1
fpn3-2
FER3
6000
4000
2000
0
FER4
3000
2000
1000
0
NRAMP4
15000
10000
5000
0
FRO7
4000
3000
2000
1000
0
FRO3
20000
15000
10000
5000
0
FRO3 (+Fe)
1500
1000
500
0
FRO8
600
400
200
0

Figure 7.

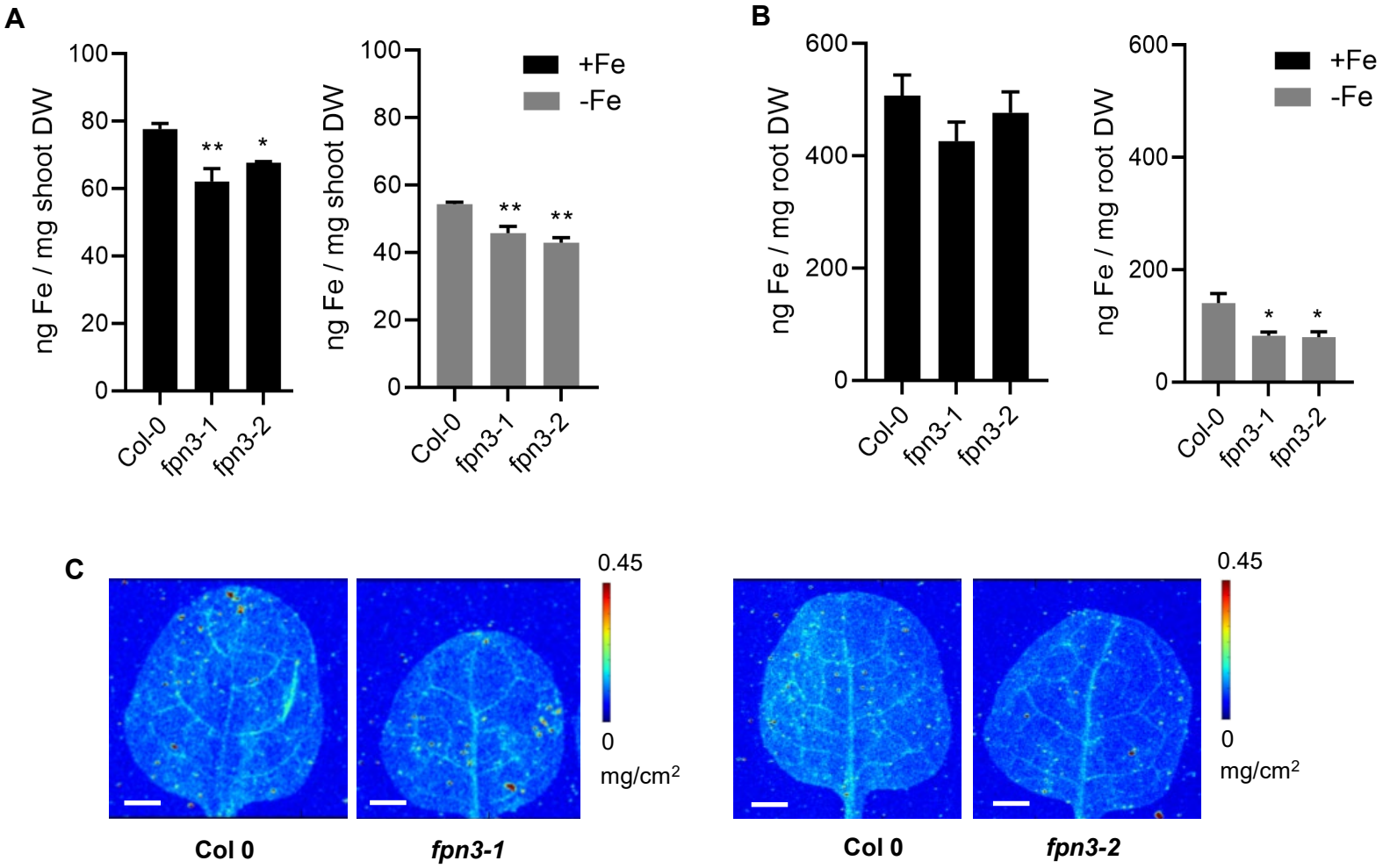
A
ng Fe / mg shoot DW
100
80
60
40
20
0
**
*
Col-0
fpn3-1
fpn3-2
+Fe
-Fe
B
ng Fe / mg root DW
600
400
200
0
C
0.45
0
mg/cm2
Col 0
fpn3-1
fpn3-2

Figure 8.

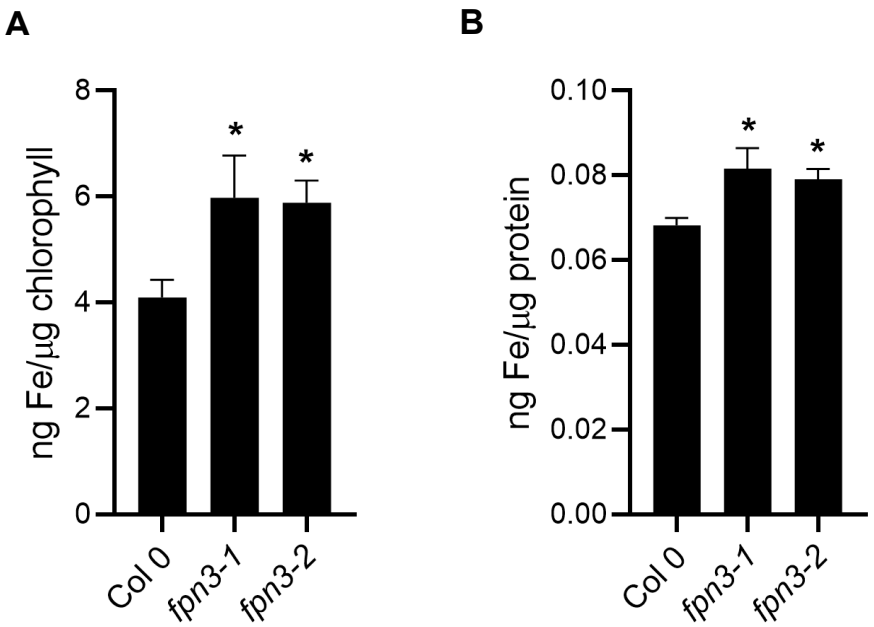
A
B
ng Fe/µg chlorophyll
ng Fe/µg protein
8
6
4
2
0
0.10
0.08
0.06
0.04
0.02
0.00
*
Col 0
fpn3-1
fpn3-2
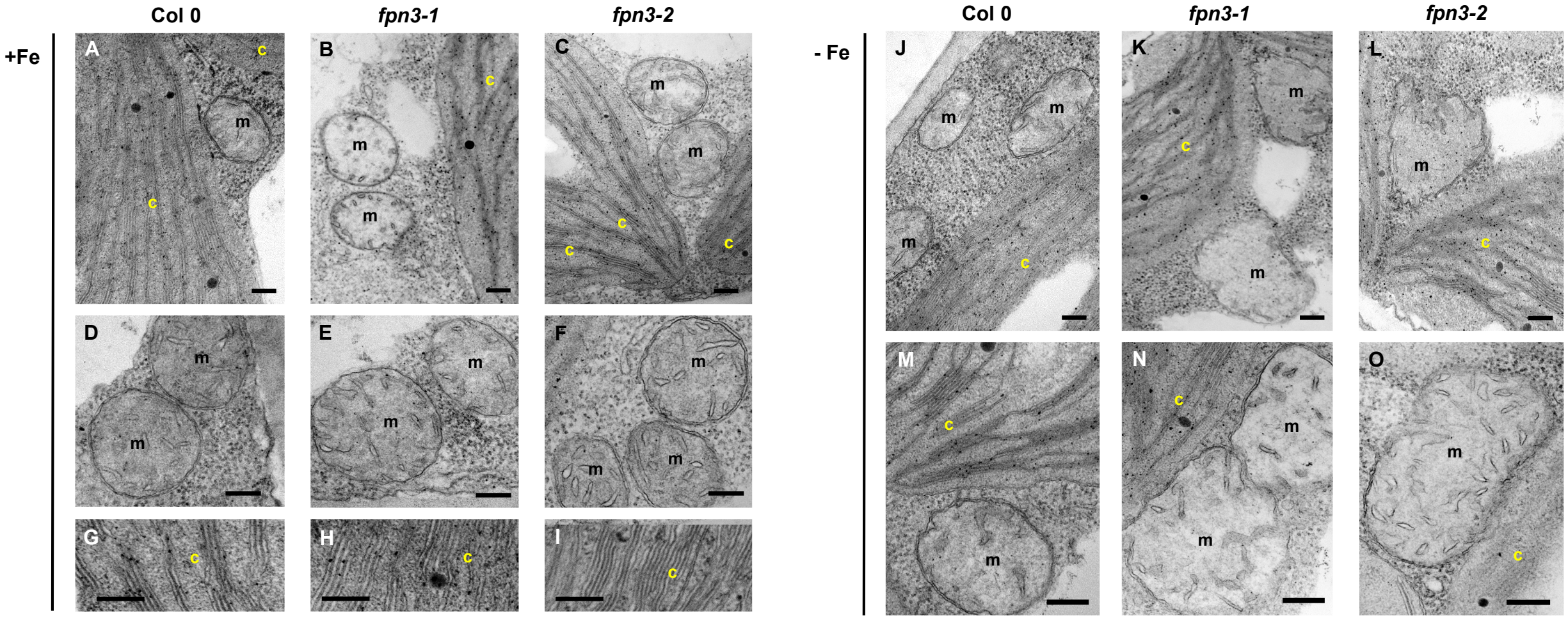
Figure 9.